Optimization-based Modeling and Economic Comparison of Membrane Distillation Configurations for Application in Shale Gas Produced Water Treatment

Elmira Mohammadi Shamlou[1], Radisav Vidic[1,2], and Vikas Khanna[1,2*]

[1] Department of Civil and Environmental Engineering, University of Pittsburgh, 3700 O'Hara Street, 742 Benedum Hall, Pittsburgh, Pennsylvania 15261, United States

[2] Department of Chemical and Petroleum Engineering, University of Pittsburgh

*Address correspondence to khannav@pitt.edu

Abstract

Membrane distillation (MD) is an emerging membrane technology with great potential for treatment of hypersaline wastewater generated by unconventional (shale) oil and gas reservoirs. However, the low energy efficiency of this technology makes the operating cost of MD systems relatively high, especially in the absence of waste heat. There are several MD configurations with inherent advantages and disadvantages and varying performance. As such, there is a need for thermo-economic optimization of MD systems in a systematic manner to assess their economic performance. We present an optimization framework to model and compare the performance of six MD configurations (DCMD, AGMD, PGMD, CGMD, SGMD, and VMD) in continuous recirculation mode for treatment of hypersaline wastewater. The optimization results show that AGMD with small gap size operated at low stream Reynolds number outperforms all other configurations with treatment cost of 4.57 US $/m^3 of feed. However, restricting the system design to more practically relevant operating conditions, such as higher Reynolds number and larger gap size, diminishes the cost superiority of AGMD over other configurations. We also

observed that treatment cost using PGMD configuration approaches those of CGMD and DCMD, particularly when modules with small gaps are used.

Keywords: Membrane distillation, continuous recirculation, optimization, produced water, desalination

1 Introduction

Desalination technologies offer great promise to provide fresh water where natural resources are limited and for treatment of wastewaters and groundwaters of varying salinities while simultaneously protecting the environment and available freshwater reservoirs. Two broad and popular categories of desalination technologies include thermal distillation (e.g. multi-stage flash distillation, multi-effect evaporation) and membrane-based desalination (e.g. reverse osmosis, forward osmosis) [1]. Large footprint, high equipment costs, and risk of material corrosion make conventional thermal distillation methods less suitable for small scale plants with high salinity feed [2, 3]. Similarly, inability of reverse osmosis to handle the high salinity of certain streams (e.g., unconventional oil and gas wastewater) makes it impractical for such applications [4]. High salt concentration, usually between 70,000 and 350,000 mg/L total dissolved solids (TDS) is characteristic of produced water generated by the unconventional oil and gas industry [5]. Flowback and produced water volume from unconventional reservoirs in the United States range between 0.5- 3.8 million gallons per well over the first 5–10 years of production [6]. If not properly managed, wastewater from shale gas production could contaminate aquifers and negatively impact biological species, soil, and vegetation due to elevated level of salinity and toxicity [7-9]. The current dominant strategy in the US for managing shale gas wastewater is injection into underground disposal wells [10, 11]. However, this strategy has limited potential in

areas with insufficient disposal wells (e.g. Marcellus shale in Pennsylvania) and has also been linked to induced seismicity [12-14] . As such, there is a need to explore and evaluate technologies for treatment of high salinity wastewaters to ensure the long-term sustainability of this industry. Membrane Distillation (MD) technology is one such promising technology for treatment of high salinity wastewaters [2].

MD is a desalination technology capable of modular design and the ability to treat hypersaline wastewater without the aforementioned drawbacks of most commonly used desalination technologies. MD combines thermal and membrane processes to utilize the difference in vapor pressure induced by a temperature gradient across a hydrophobic membrane. The vapors produced from the preheated feed (usually between 40-90^{o}C) traverse through the microporous membrane and are collected and condensed in various ways depending on the MD configurations [15]. The lower operating temperature of MD compared to other thermal desalination technologies makes it uniquely suited for integration with waste heat sources [16]. Despite the unique advantages of MD, it suffers from low single pass recovery (i.e., maximum of 10% [17]) that impacts the operational mode and design of the system. Batch recirculation and continuous recirculation modes of operation can overcome this limitation [17-19]. With batch operation mode, a certain amount of feed in the circulation tank is sent to the membrane multiple times until the salinity of the feed in the tank reaches a desired level. Although batch operation mode is shown to have better energy efficiency than other recirculation modes [18], such unsteady state operation may not be suitable for large scale or continuous operations [19]. Continuous recirculation is a steady state operation mode in which input feed (makeup) to the system is mixed with comparatively large portion of the membrane reject brine (recycle stream) and the resulting mixed stream is sent to the membrane unit for water recovery. The ratio of recycle

stream flowrate to makeup feed flowrate, recycle ratio, is dependent on membrane configuration, design, and energy performance of the system.

Lokare et. al [17] estimated the recycle ratio of the DCMD system for various recoveries and showed that operating in continuous recirculation mode significantly increases the thermal energy demand to heat both the makeup feed and the large volume of recycle stream. In another study [18], Swaminathan and coworkers demonstrated that the performance of MD systems is negatively impacted by vapor pressure depression caused by the system's increased operating salinity in continuous recirculation mode. Thus, when analyzing MD systems for high recovery applications (e.g., produced water desalination or zero liquid discharge (ZLD)), it is critical to analyze their performance in continuous recirculation mode instead of single pass in order to obtain accurate estimate of the desalination system's cost and energy performance.

MD configurations commonly discussed in the literature include Direct contact (DCMD), air gap (AGMD), permeate gap (PGMD), conductive gap (CGMD), sweeping gas (SGMD), and vacuum (VMD) membrane distillation [20-22]. Each configuration has its own set of advantages and disadvantages that vary according to the application and operating conditions of the process. Multiple previous studies have reported performance metrics in comparative evaluations of MD configurations [23-30]. However, most studies have focused primarily on the effect of system operating conditions on energy efficiency, flux, or energy consumption, without accounting for the tradeoffs between cost and the aforementioned parameters in order to achieve optimal MD design. Several studies have also assessed MD systems from a technoeconomic perspective as a function of feed salinity and water recovery [31-38]. These studies have evaluated the economic and energetic performance of specific types of MD configurations without a formal comparison of different configurations under consistent specifications (e.g., input salinity, water recovery,

operation mode, membrane and plant characteristics). Because the estimation of an MD system's economic and technical performance is highly dependent on the assumptions made in a study, a formal optimization-based comparison is required to evaluate the technoeconomic feasibility of various MD configurations within a consistent framework.

We present an optimization-based model to evaluate the technical and economic performance of DCMD, AGMD, PGMD, CGMD, VMD, and SGMD configurations in continuous recirculation mode. The developed optimization models are utilized to compare the treatment costs and energy consumption of different MD configurations for treatment of hypersaline feed and high water recovery applications, such produced water from unconventional reservoirs and ZLD processes. Additionally, we provide an in-depth analysis of various performance metrics for selected configurations along with discussion of theoretically optimal versus practically relevant design of MD systems. Finally, we investigate the effect of feed and concentrate (i.e., reject brine) salinity, inlet temperature, feed channel turbulence, gap size in gap type MD systems, and membrane thickness on the performance of various MD configurations. To the best of our knowledge, this is the first optimization-based study to provide a comprehensive comparative evaluation of all MD configurations from a cost, energy, and practical perspective.

2 Methodology

2.1 Process Description

DCMD and gap type MD configurations (including AGMD, PGMD, and CGMD) include a hot flow channel and a cold channel across a hydrophobic membrane. The cold channel in DCMD is in direct contact with the membrane surface, whereas there is a gap between the cold channel and the membrane surface in gap type MD. In AGMD, the gap is filled with air and

woven polymer spacers; In PGMD, the gap is filled with water and woven polymer spacers; And in CGMD, the gap is filled with water and conductive materials [24]. The cold channel is replaced in SGMD and VMD by an air and vacuum channel that is in direct contact with the membrane surface. Permeation, condensation, recirculation, cooling, preheating, and heating are the five stages in a typical membrane distillation process and are discussed below.

Permeation. Figure 1(a-d) illustrates the continuous recirculation mode of operation for DCMD, AGMD, PGMD, CGMD, SGMD, and VMD. The hot feed from the heater enters the membrane's hot channel. Water vapor permeates the hydrophobic membrane pores due to the vapor pressure difference across the membrane. The vapor pressure on the membrane surface on the hot channel side is a function of the vapor saturation temperature in all configurations. In DCMD, PGMD, and CGMD, the vapor pressure difference is a function of the vapor saturation temperature gradient across the membrane. Similarly, the vapor pressure differential in AGMD is proportional to the difference in vapor saturation temperature between the hot channel membrane surface and the cooling wall surface. However, in SGMD, the vapor pressure in the air channel depends on the vapor content (humidity ratio) of the air, which may or may not be saturated. *It should be noted that in this study, sweeping gas is assumed to be air, and the terms will be used interchangeably throughout this manuscript*. In VMD, the vapor pressure in the vacuum channel is equal to the applied vacuum pressure.

Condensation. In DCMD, permeated water condenses on the water surface on the cold channel since there is no gap between the cold channel and the membrane. The permeated vapor in AGMD passes through the airgap and condenses on the cooling surface, forming a condensing film. Because the gap in PGMD and CGMD is filled with water, the permeated vapor condenses

on the water in contact with the membrane surface as soon as it exits the membrane pores. In SGMD and VMD, moist air and vapor flow to an external condenser for permeate condensation.

Recirculation. In continuous recirculation mode, a significant portion of the brine leaving the membrane unit is recirculated and mixed with the incoming feed, while a small portion exits the system as reject brine.

Cooling. In DCMD, the pure water flow exiting the module's cold channel enters a heat exchanger followed by a chiller to maintain the temperature difference across the membrane. In gap type MD configurations, the recirculating brine is cooled before entering the cold channel via a chiller to maintain the required temperature difference for permeation and condensation. Similarly, the recirculating brine in SGMD passes through a chiller before entering the condenser to provide the required cooling for condensation. In VMD, coolant exiting the condenser enters the chiller to meet the condenser's cooling demand.

Preheating and heating. In DCMD, only pure water may be used as a coolant because permeate condenses on the cold channel, necessitating the use of an external heat exchanger to recover heat from the heated coolant thereby pre-heating the feed. Similarly, in SGMD, the recirculating brine and makeup feed are preheated by routing them through an external condenser. Because all gap type membranes (AGMD, PGMD, CGMD) have separate permeate and cold channels, the feed (a mixture of cooled recirculating brine and makeup feed) can be used as the coolant in the cold channel, recovering heat directly from the hot side of the membrane. In VMD, the temperature of the recycle stream at the module's exit is always greater than the temperature of the vapor on the vacuum side. As a result, no effective heat recovery is possible in the external condenser for the recycle stream and only the low-temperature makeup

feed will recover some heat by passing through the external condenser. The VMD's recirculating brine bypasses the chiller and flows directly into the heater.

a)

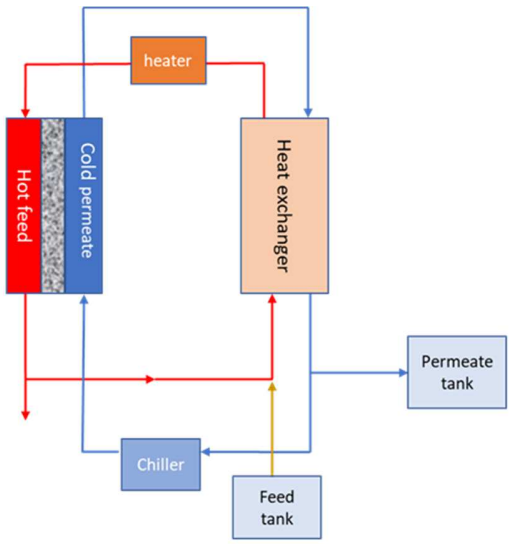

b)

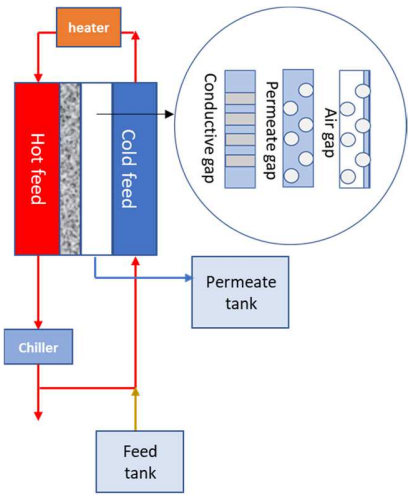

c)

d)

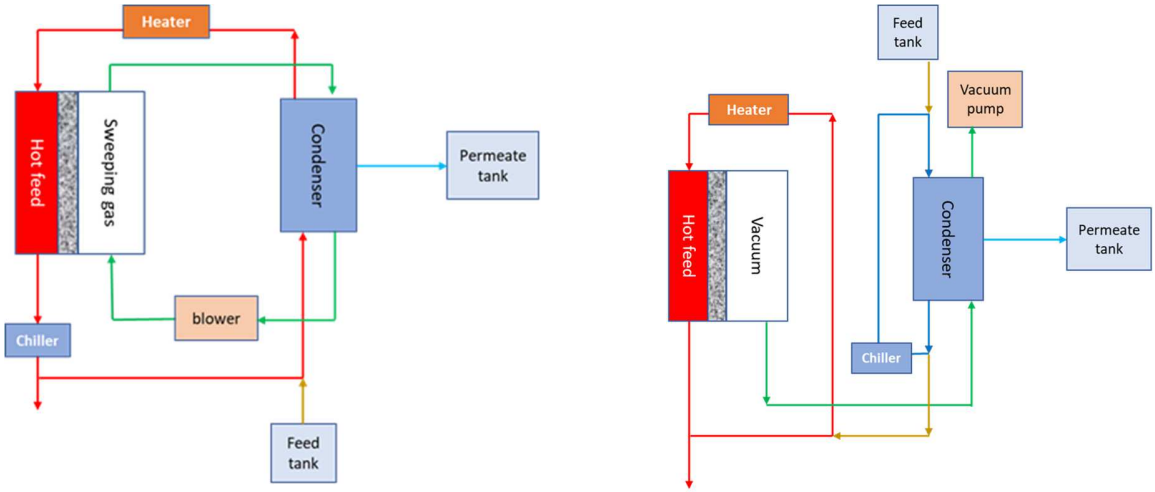

Figure 1. Membrane distillation configurations in single stage continuous recirculation operation mode:

a) DCMD, b) Gap type MD, c) SGMD, d) VMD

2.2 *Optimization model description*

For each membrane configuration, the optimization model incorporates the governing thermodynamic processes as equality and inequality constraints. This model is expressed as a nonlinear programming problem with the objective of minimizing the total cost of treated produced water for a given recovery:

$$\min \mathrm{TUC}\,(y), y = (T, M, X)^T \in \mathbb{R}$$

$$\text{s.t.} \quad \varphi(y) = 0$$

$$\psi(y) \leq 0$$

Temperature, salinity, and flowrate of all streams are independent variables to optimize, while recirculation ratio, total membrane area, module length and width, heat exchanger and condenser total area, required heating steam, chilling energy, and pumping energy are dependent variables.

It should be noted that in our initial optimization models, we entered membrane thickness as a constant parameter and used one of the commercially available membranes with a known permeability coefficient and active layer thickness of 0.06mm (Appendix table A2 contains a comprehensive list of membrane properties) [39]. However, in order to investigate the effect of membrane thickness on treatment costs, we performed a second round of optimization with membrane thickness as one of the variables to be optimized:

$$\min \mathrm{TUC}\,(\mathrm{y}), \mathrm{y} = (\mathrm{T}, \mathrm{M}, \mathrm{X}, \delta_{\mathrm{m}})^{\mathrm{T}} \in \mathbb{R}$$

$$\text{s.t.} \quad \varphi(\mathrm{y}) = 0$$

$$\psi(\mathrm{y}) \leq 0$$

We assume that all configurations operate at steady state and heat loss in equipment is negligible. It is assumed that permeate exits the membrane pores with zero salinity. Additionally, we assume that film gravitational condensation occurs in the airgap for AGMD configuration. The optimization problem in this study is solved using the General Algebraic Modeling (GAMS) software and the local solver CONOPT [40].

2.3 Modelling membrane distillation process

To model large-scale modules, each membrane module is divided lengthwise into a number of slices and mass and energy balances are established for each slice. This section will outline the general structure of heat and mass transfer in the membrane distillation process. The detailed equations and correlations used to model each type of MD configuration are summarized in the appendix in tables A.5- A.7.

The permeability coefficient and pressure difference across the membrane determine the mass flux through each slice (Equation 1).

$$J^z = B\Delta p^z \qquad \forall\, z \in Z \qquad (1)$$

The mass change along each slice of the hot channel is proportional to the area of the slice and the mass flux (Equation 2).

$$\Delta M^z = -J^z \Delta A^z \qquad \forall\, z \in Z \qquad (2)$$

The mass change along the cold channel is determined by whether or not the cold channel receives permeate. The flowrate along the cold channel does not change in the gap MD configuration, but it changes in the DCMD, VMD, and SGMD configurations as shown in Equation 3.

$$\Delta M^z = J^z \Delta A^z \qquad \forall\, z \in Z \qquad (3)$$

As no salt passes through the membrane, the absolute mass of salt along the hot channel remains constant while concentration varies from the inlet to exit (Equation 4).

$$\Delta M^z X^z = 0 \qquad \forall\, z \in Z \qquad (4)$$

Convection heat transfer occurs through cold and hot channels, while various combination of evaporation and conduction heat transfer occurs through intermediate channels. The convective heat transfer coefficient is used to estimate convective heat flux, and the thermal conductivity and thickness of the heat transfer medium are used to calculate conduction heat flux (Equations 5 and 6).

$$q^z_{conv} = h^z(\Delta T^z) \qquad \forall\, z \in Z \qquad (5)$$

$$q^z_{cond} = \frac{k}{\delta}(\Delta T^z) \qquad \forall\, z \in Z \qquad (6)$$

The evaporative heat flux is proportional to the mass flux and enthalpy of evaporation (Equation 7)

$$q_v^z(T) = J^z H_v^z(T) \qquad \forall\, z \in Z \qquad (7)$$

where,

$$H_v^z(T) = H_{sl}^z(T) + H_e^z(T) \qquad \forall\, z \in Z \qquad (8)$$

The enthalpy change along each slice of the cold and hot channel is proportional to the convective heat flux and area of the slice (equation 9)

$$M^z \Delta H^z = q_{conv}^z \Delta A^z \qquad \forall\, z \in Z \qquad (9)$$

2.4 Performance measurement criteria

Several performance criteria are used in this work to compare the performance of various MD configurations and are described below.

Gain output ratio, thermal efficiency, and energy recovery. The gain output ratio (GOR), is a measure of a desalination system's thermal energy performance. It is defined as the ratio of the total heat of permeate evaporation to the total heat of consumed steam (Equation 10).

$$GOR = \frac{\sum_z q_{v_z}}{Q_s} = \frac{\sum_z M_{p_z} h_{v_z}}{M_s h_{v_s}} \qquad (10)$$

GOR is dependent on the thermal efficiency (η_{th}) and heat recovery ratio (HR) of MD systems. The thermal efficiency (Equation 11) of a membrane is defined as the ratio of the total enthalpy of the permeated vapor to the total heat transferred across the membrane (Q_t):

$$\eta_{th} = \frac{\sum_z q_{v_z}}{Q_t} = \frac{\sum_z q_{v_z}}{\sum_z (M_{p_z} h_{v_z} + q_{v_z})} \qquad (11)$$

The overall heat recovery ratio is defined as the ratio of total heat recovered within the MD system to total heat consumed for separation (which is the sum of heat recovered and external heat of steam):

$$\mathrm{HR_{overall}} = \frac{\mathrm{Q_{HR}}}{\mathrm{Q_{HR}+Q_s}} \tag{12}$$

The heat recovery ratio within the MD module is defined as the ratio of heat recovered by the MD's cold channel flow to total heat consumed for separation:

$$\mathrm{HR_{MD}} = \frac{\mathrm{Q_t}}{\mathrm{Q_{HR}+Q_s}} \tag{13}$$

The heat recovered in AGMD, CGMD, and PGMD systems with direct heat recovery is equal to the total heat transferred through the membrane ($\mathrm{Q_{HR}} = \mathrm{Q_t}$, and $\mathrm{HR_{overall}} = \mathrm{HR_{MD}}$). In DCMD and SGMD systems with external heat exchangers for heat recovery, the heat recovered is equal to the heat transferred through the heat exchanger. ($\mathrm{Q_{HR}} = \mathrm{Q_{hx}}$, and $\mathrm{HR_{overall}} = \mathrm{HR_{MD}}\frac{\mathrm{Q_{hx}}}{\mathrm{Q_t}}$). For systems with insignificant heat recovery, such as VMD configuration considered in this study, the total heat transferred through the membrane is almost equal to the total heat of steam ($\mathrm{Q_t} \sim \mathrm{Q_s}$). This is especially true when the recycle stream flowrate is high in comparison to the makeup feed flowrate in VMD. By combining equations 10- 13, and defining the external heat recovery factor as ($\mathrm{f_{hx}} = \frac{\mathrm{Q_{hx}}}{\mathrm{Q_t}}$)we obtain the following:

$$\mathrm{GOR} = \eta_{\mathrm{th}}\frac{\mathrm{Q_t}}{\mathrm{Q_s}} \tag{14}$$

$$\mathrm{GOR}\begin{cases} = \eta_{\mathrm{th}}\frac{\mathrm{HR}}{1-\mathrm{HR}} & \text{for AGMD, PGMD, and CGMD} \\ = \eta_{\mathrm{th}}\frac{\mathrm{HR_{MD}}}{1-\mathrm{f_{hx}HR_{MD}}} & \text{for DCMD and SGMD} \\ \sim \eta_{\mathrm{th}} & \text{for VMD} \end{cases} \tag{15}$$

In the remainder of this analysis, we will refer to the overall heat recovery ratio as the heat recovery ratio, and the above equations were developed solely to illustrate the relationship between the GOR, the heat recovery ratio, and the thermal efficiency.

Recovery Ratio and single pass recovery ratio: The recovery ratio (RR) is defined as the ratio of permeate production to the system's makeup feed flowrate (Equation 16). Single pass recovery (SPR) is defined as the ratio of permeate production to total input feed to the MD module, i.e. recycle stream plus makeup feed (Equation 17).

$$\mathrm{RR} = \frac{\sum_z \mathrm{M_{p_z}}}{\mathrm{M_f}} \tag{16}$$

$$\mathrm{SPR} = \frac{\sum_z \mathrm{M_{p_z}}}{\mathrm{M_f + M_{rec}}} \tag{17}$$

Recycle ratio is defined as the ratio of the recycle stream to the input makeup feed (Equation 18).

$$\mathrm{RecR} = \frac{\mathrm{M_{rec}}}{\mathrm{M_f}} \tag{18}$$

The specific area of a membrane is defined as the area of the membrane per unit mass of feed entering the MD module (Equation 19).

$$\mathrm{A_s} = \frac{\mathrm{A_t}}{\mathrm{M_{rec} + M_{rec}}} \tag{19}$$

3 Results and Discussion

The optimization model is applied for a hypothetical produced water treatment plant with a treatment capacity of 10 kg/s (~0.25 million gallons per day), concentrating produced water with 10% (100,000 mg/Liter) TDS to brine with 30% TDS corresponding to saturation conditions to

make the system capable of integration with crystallizers for ZLD operation. The model input parameters, including plant characteristics, membrane properties, and capital and operating cost data, are provided in Tables A.1 to A.4. in the Appendix.

3.1 Treatment cost

Figure 2a shows a comparison of the produced water treatment cost obtained from the optimization model for the studied MD configurations. AGMD outperforms all other configurations with \$4.57/m^3_{feed} treatment cost followed by CGMD, DCMD, SGMD, VMD, and PGMD with 7.8, 8.7, 9.8, 11.63, and 24.61\$/m^3_{feed}, respectively. The operating cost accounts for the majority of the total treatment cost and is the primary reason for treatment cost differences across configurations. Energy costs for heating and cooling are the two largest components of operating costs (Appendix Table A.8). DCMD and SGMD have the highest capital costs, followed by PGMD, CGMD, AGMD, and VMD. The high capital cost of DCMD and SGMD is primarily due to the large surface area external heat exchanger and condenser, respectively. DCMD also has a relatively high installation cost because it has two separate loops with high flowrates for the cold and hot sides. The chiller and installation costs account for the largest share of the PGMD relatively high capital cost because of the high recycle stream flowrate. The membrane cost is a significant component of the AGMD and CGMD capital costs with AGMD requiring large area and CGMD with expensive conductive material. Among all configurations, VMD with small membrane area, small condenser surface area, and low recycle stream flowrate has the lowest capital cost. It is worth noting that we assumed that complete condensation occurs in the external condenser of the VMD. As a result, the vacuum pump removes only non-condensable gases, resulting in a negligible vacuum pump operating and capital cost in comparison to other cost components.

It is worth noting that we assumed the price used for heat exchanger to be applicable to the conductive material filling per unit of area. Accurate cost estimate for conductive materials suitable for CGMD application is necessary and should be studied in the future. Conductive filling materials include metal mesh, metal foam, and finned plate. Metal mesh is ineffective because it does not increase conductivity to the levels considered in this study. Metal foams are also extremely costly and the conductive material assumed in this study is finned plate and has been tested previously [21]. Furthermore, the material and cost of the condenser in SGMD and VMD are assumed to be identical to those of the metal plate and frame heat exchanger. Alternative materials (e.g. plastics) and dehumidifiers with innovative designs [41, 42] could offer the potential to lower costs and should be investigated in future studies.

3.2 Flux and total membrane area

The operating flux and total membrane area of the studied membrane configurations corresponding to their lowest treatment cost are shown in Figure 2b. With the largest membrane area, AGMD has the lowest flux of 2.1 L/hr/m^2 (LMH), while VMD and DCMD with lowest membrane areas have the highest fluxes of 14.6 and 12.8 LMH, respectively. The maximum salinity at the membrane interface is set to 30 % for modeling purposes to prevent oversaturation due to concentration polarization. As a result, the maximum operating flux of each MD configuration is constrained by the concentration polarization, which is determined by the hot channel flow Reynolds number. This is particularly important in applications where MD works at high salinities, such as the ZLD condition studied here.

a) b)

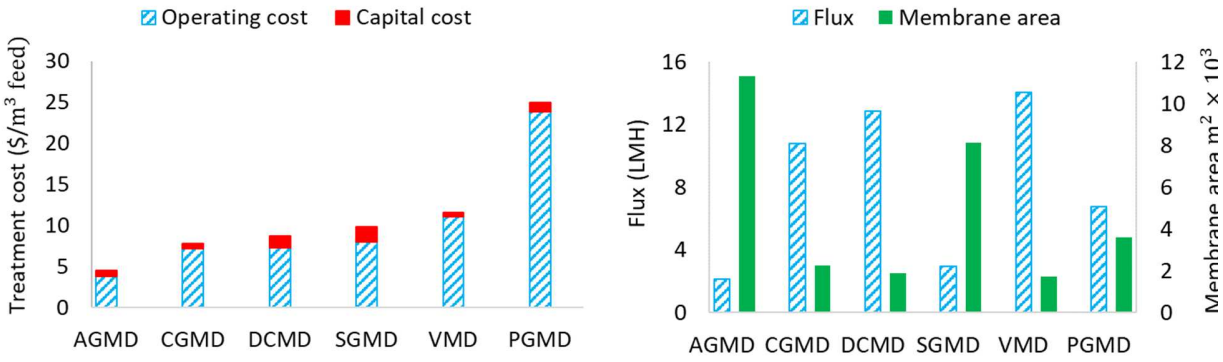

Figure 2. Treatment cost, flux and total membrane area for cost optimal design

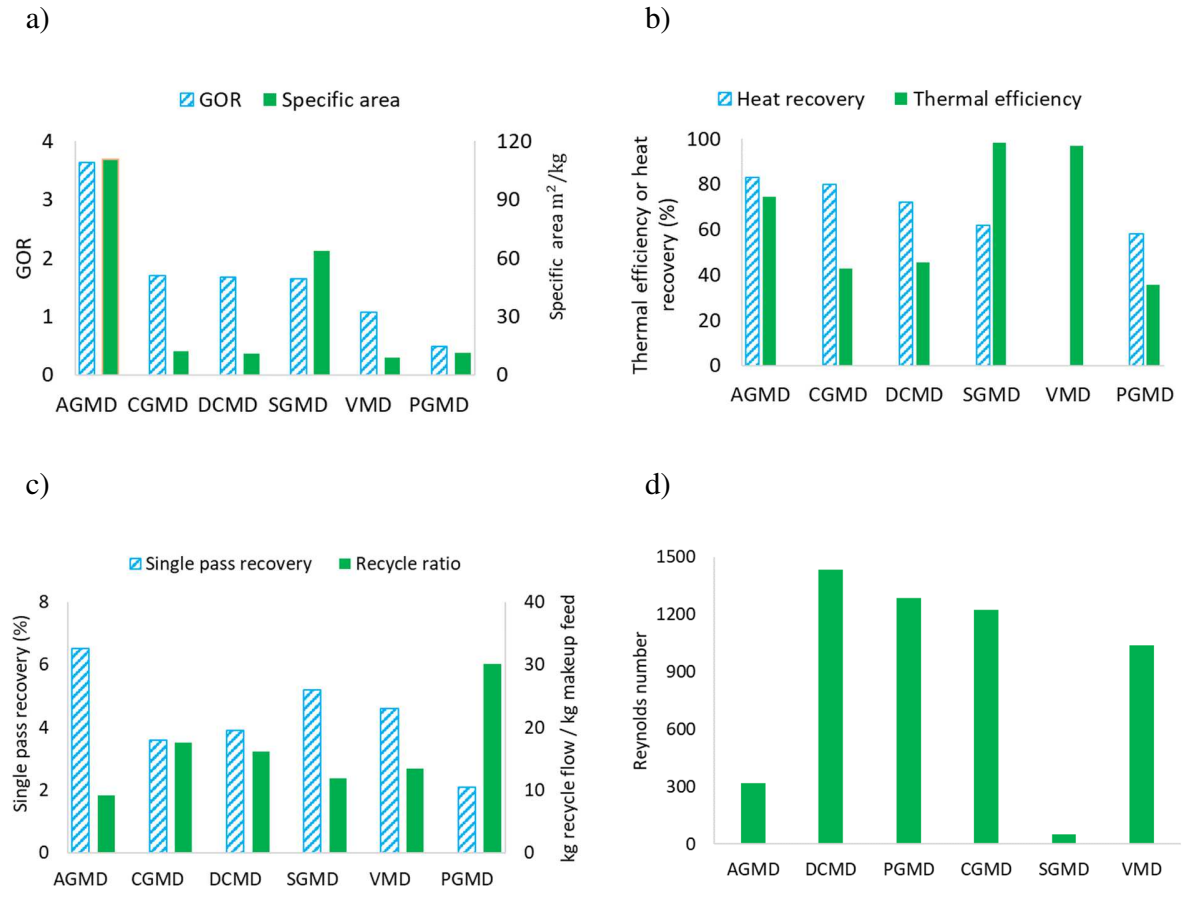

Figure 3. Performance metrics for cost optimal design: a) GOR and specific area, b) Thermal efficiency and heat recovery, c) Single pass recovery and recycle ratio, d) Hot channel Reynolds number

3.3 GOR and specific area

The GOR and specific area for the studied MD configurations are shown in Figure 3a. The energy consumption in MD systems is inversely proportional to their GOR, and systems with higher GOR have lower heating and cooling costs. AGMD with a GOR of 3.6 has the best energy performance, while PGMD with a GOR of 0.5 shows the lowest energy performance among all MD configurations. The GOR is governed by the thermal efficiency and energy recovery of the MD systems, both of which depend on the membrane specific area and heat and mass transfer resistance through membrane channels. Specific area is an indicator of optimum area for heat and mass transfer per unit mass flowrate through the hot channel. Unlike total membrane area, specific area is unaffected by plant capacity or recycle ratio, making it easier to compare the energy performance of different MD systems. For example, despite having a significantly larger total membrane area than DCMD, CGMD, and VMD, PGMD has roughly the same specific area as these configurations. Except for the VMD configuration, higher specific area results in greater energy recovery and lower thermal efficiency, resulting in a specific area with a unique combination of thermal efficiency and energy recovery that yields the highest GOR [24]. When minimizing the total unit cost of the system, the obtained optimum specific area is influenced by the tradeoff between membrane cost, pump cost (or blower cost in the case of SGMD), and GOR (corresponding to steam cost).

3.4 Thermal efficiency and heat recovery

Figure 3b shows the thermal efficiency and overall heat recovery for the lowest treatment cost for the six MD configurations. In the following section, we will investigate the primary

cause of the difference in energy performance of various MD configurations by comparing each configuration's thermal efficiency, heat recovery, and specific area to others.

3.4.1 VMD

The highest thermal efficiency is achieved by VMD due to its vacuum channels, which prevents heat conduction. As previously stated, there is insignificant heat recovery in the VMD module when operating in single stage continuous recirculation mode, and its GOR is approximately equal to the system's thermal efficiency. As a result, VMD achieves a relatively low GOR in comparison to other configurations (excluding PGMD) with higher heat recoveries. The underlying reason for poor performance of PGMD will be explained in detail in subsection 3.4.5.

3.4.2 AGMD

Following VMD, SGMD and AGMD have the highest thermal efficiency due to their air channels that limit heat conduction. Although both AGMD and SGMD have air channels, AGMD has slightly lower thermal efficiency than SGMD because: 1) AGMD has larger membrane area with lower average temperature difference across the module, 2) sweep gas in SGMD is not always saturated along the module, and evaporation in this module is not always a function of saturation temperature, which is affected by module size, and 3) SGMD has lower mass transfer resistance than AGMD because of the sweep gas flow.

The design of an AGMD system is primarily affected by the trade-off between membrane cost, pumping cost, and steam cost. The high thermal efficiency and mass transfer resistance in AGMD make it possible to operate with large specific area and low flux, resulting in relatively high energy recovery and the highest GOR among other configurations. By operating at specific

areas larger than the cost optimum specific area, AGMD can achieve higher GOR than the cost optimum GOR (shown in figure 3a). Membrane and pumping costs, however, limit operation in large specific areas.

3.4.3 SGMD

SGMD has a lower GOR than AGMD, despite having a higher thermal efficiency. This is primarily due to the limited heat recovery in SGMD compared to the AGMD. The optimum design of SGMD is primarily influenced by the tradeoff between blower, condenser, and steam costs. The amount of steam consumed is inversely proportional to the amount of heat recovered within the external condenser. Heat transfer and heat recovery in the condenser for SGMD configuration are dependent on the sweep gas temperature, which has a direct effect on the cost of the condenser via the terminal temperature difference. The convective heat transfer coefficient of air flow is low, and vapor flux condensation occurs primarily outside the membrane module in the condenser, resulting in slow temperature rise for air along the module. The amount of temperature rise in the sweep gas is determined by the membrane area and the air flow convective heat transfer coefficient, which is directly linked to the air flow Reynolds number. Higher Reynolds numbers for air flow, on the other hand, translate to higher blower costs. As a result, SGMD operate over large membrane areas and low air flow Reynolds numbers. This has the benefit of reducing steam consumption by allowing the air to be effectively humidified and heated while avoiding the high capital and operating costs associated with condensers and blowers.

We observe that the optimal ratio of hot channel (feed) to air channel flowrate is 4.6. Higher flowrate ratios than the optimum ratio will reduce GOR because the temperature change in the hot feed flow in both the module and the external condenser will be lower, limiting the heat

recovery ratio in the SGMD. Lower flowrate ratios also have a negative impact on system cost by increasing the cooling requirement for external condensation due to the smaller volume of water.

3.4.4 DCMD and CGMD

Because CGMD and DCMD have lower mass transfer resistance and lower thermal efficiency than AGMD, these configurations achieve slightly lower heat recovery with relatively smaller specific areas and higher flux. The higher thermal efficiency of AGMD compared to CGMD and DCMD also results in a significantly higher GOR, more than twice that of CGMD and DCMD.

DCMD and CGMD have lower thermal efficiency and higher heat recovery in comparison to SGMD, resulting in nearly identical GOR for all three configurations. However, despite having similar GOR, SGMD has a higher treatment cost than DCMD and CGMD due to the condenser capital cost and blower operating cost.

DCMD has slightly higher thermal efficiency with slightly lower heat recovery than CGMD, but they both produce roughly the same GOR. The conductive gap channel causes slight temperature increase on the condensation surface in CGMD, resulting in lower thermal efficiency compared to DCMD. In comparison to CGMD, DCMD suffers from an external heat exchanger with large surface area (~4 times the membrane area in this study) and high capital cost, resulting in lower heat recovery ratio. However, DCMD has two advantages that compensate for the limited heat recovery in the external heat exchanger, resulting in the same GOR as CGMD for the cost-optimal design: 1) The hot brine at the module exit is not cooled by a chiller in DCMD resulting in a lower total heat (external steam plus recovered heat) required for the separation process, and 2) Unlike gap type MD configurations, DCMD has a degree of

freedom on the cold (permeate) side flowrate, which need not be equal to the hot side stream flowrate. It has been argued previously that for single pass DCMD, the ratio of cold to the hot side flowrate has an important role in optimum performance of MD system [43]. Low flowrate ratios are associated with a rapid rate of temperature change on the cold side, limiting mass transfer along the DCMD module, while high flowrate ratios are associated with a slow rate of temperature change on the cold side, limiting heat recovery in the external heat exchanger. For the specified operating conditions in this study, the analysis shows that the optimum cold side to hot side inlet flowrate ratio for DCMD in continuous recirculation mode is 0.79. Increasing the flowrate ratio from 0.79 to 1 for DCMD (as in gap MD configurations) has a negative impact on system performance, resulting in a 22% reduction in GOR and an 18% increase in total treatment cost. This is mainly because at higher flowrate ratio, the increase in cold side temperature is lower which results in smaller terminal temperature difference in the heat exchanger for higher heat recoveries. Further, the high capital cost of heat exchanger at higher flowrate ratio limits heat recovery in a cost-optimal design, resulting in lower GOR and higher cost.

3.4.5 PGMD

While PGMD has comparable specific area to DCMD and CGMD, it has lower thermal efficiency and heat recovery. This is because the condensation surface in PGMD is at the interface of permeate gap and membrane. The permeate gap serves as an additional heat resistance layer between the condensation surface and the coolant channel. As a result, the saturation temperature and pressure on the PGMD condensation surface increase, while the average temperature difference across the membrane decreases, resulting in a reduction in both thermal efficiency and heat recovery. This also explains why adding conductive material to CGMD or eliminating the gap in DCMD improves thermal efficiency and heat recovery when

compared to PGMD. Additionally, VMD with minimal heat recovery (exclusively via makeup feed) has a higher GOR than PGMD with heat recovery. This is because VMD has a significantly higher thermal efficiency across the module's length than PGMD. The detrimental effect of liquid gap on PGMD thermal efficiency is more pronounced at the studied reject brine salinity of 30% and membrane thickness of 60 micrometer. This is described in greater detail in the sub-section on brine salinity and thickness analysis.

3.5 Recycle ratio and single pass recovery

The recycle ratio for all configurations is determined by the single pass recovery (SPR) and the total desired water recovery. Figure 3c illustrates the optimal SPR and recycle ratio for each configuration in order to achieve the target recovery of 67 percent (final brine salinity of 30 percent). All MD configurations have a very low SPR (maximum 6.5 percent for AGMD), and this translates into high recycle ratio to achieve the desired recovery. Additionally, the results indicate that the configurations with highest thermal efficiency AGMD, SGMD, and VMD have the highest single pass recovery and the lowest recycle ratio. Along with increased heating and cooling demand, a high recycle ratio increases the cost of pumping electricity as well as capital costs for equipment such as membranes, chillers, heat exchangers, and installation. This effect is noticeable in the capital and operating costs of the PGMD with the highest recycling ratio.

3.6 Reynolds number

Different MD configurations operate at different Reynolds numbers (Figure 3d) at their theoretical minimum treatment cost. To achieve the lowest cost, SGMD and AGMD, operate at low Re of 50 and 317, respectively. While lower Re result in higher temperatures and concentration polarization, these configurations achieve their theoretical minimum treatment cost

by operating under these flow conditions. Several studies, however, have shown a direct link between increased fouling and scaling and reduced flux when operating at low Re [44-46]. As a result, operating these configurations at such low Re may be impractical. To gain insights on practically relevant costs, we examined SGMD and AGMD systems at higher Re. Table 1 compares the obtained treatment costs for operation at Re's of 500, 1000, and 1500 to the ideal minimum cost associated with low Reynolds numbers.

Table 1. Treatment cost ($/m$^3_{feed}$) for various Reynolds number

Re	Optimum Re*	500	1000	1500
AGMD	4.57	4.65	5.55	7.22
SGMD	9.81	22.4	37.5	53.1

* The optimum Re values for AGMD and SGMD that result in the minimum cost (as specified in figure 3d) are 317 and 50, respectively.

Increasing the Reynolds number for AGMD from 317 (corresponding to lowest treatment cost) to 1500 results in a nearly 58 percent increase in the treatment cost. This is because AGMD requires large specific area (110.705 m^2/kg) to achieve the cost optimum GOR (Figure 3a). At such large specific areas, the required energy for pumping is highly dependent on the module's length to width ratio. As this ratio increases, the Reynolds number and module length increase, resulting in an increase in pressure drop and required energy for pumping. To achieve the lowest cost and high GOR while operating at large specific areas, the optimal design would have a low length to width ratio to avoid high pumping costs. At higher Reynolds number, the module

length to width ratio increases and results in higher pumping cost. In order to avoid high pumping costs at high Reynolds number, the system must operate at lower specific areas (49 m^2/kg corresponding to Reynolds number of 1500), lowering the GOR while increasing steam consumption and total treatment costs.

The variation in treatment cost with increase in Reynolds number is even more pronounced for SGMD. As previously described, blower cost is a significant component of treatment cost for SGMD systems. To achieve the lowest treatment cost and optimum GOR, SGMD has a large specific area (63.4 m^2/kg; Figure 3a). This requires the system to operate at low length-to-width ratios in order to avoid high blower costs, which dramatically reduces the Reynolds number on the feed side. While the hot channel flowrate is 4-5 times that of the air channel, its Reynolds number is an order of magnitude lower than that of air channel because of the difference in viscosity and density of the two flow streams. As a result, when the minimum allowable Reynolds number on the feed side is increased, the system must either operate at the optimal specific area but with increased length to width ratios, increasing blower costs, or with a smaller specific area, lowering the GOR and increasing steam consumption. When the Reynolds number is increased from 50 (corresponding to lowest treatment cost) to 1500, the combination of above two effects results in a 441 percent increase in treatment cost. It is worth noting that the air channel thickness in this study is comparable to the cold channel thickness in other configurations (i.e., 1.9 mm). At the same air flowrate, the lower the thickness, the greater the air side Reynolds number, pressure drop and blower cost. Increasing the air channel thickness is one way to reduce SGMD costs while decreasing the specific areas and increasing feed side Reynolds number. Although increasing the thickness of the air channel reduces the convective heat transfer coefficient, the cost savings associated with the reduced blower cost outweigh the

temperature polarization in the air stream. For example, increasing the air channel thickness from 1.9 mm to 1.9 cm reduces the cost of SGMD treatment from 53.1 to 14.9 $/m$^3_{feed}$ when operating at a minimum Reynolds number of 1500.

3.7 Sensitivity Analysis

This section investigates the variation in treatment cost as a function of hot channel inlet temperature, feed salinity, and reject brine salinity. Additional sensitivity analysis with regard to cost data and membrane properties is provided in the appendix (figure A1 and A2).

3.7.1 MD inlet temperature

The optimization model in our work has an upper bound for MD hot side inlet temperature set to 90°C, with medium pressure steam at 140°C as the heat source. The results presented in Figures 2 and 3 indicate that all membrane configurations operate at the maximum inlet temperature of 90°C in order to achieve the lowest treatment cost. MD can operate at lower temperature if a high-quality heat source is not available. Additionally, salt solubility varies with temperature, with salts such as $CaCO_3$, $CaSO_4$, and $Mg(OH)_2$ exhibiting decreased solubility at higher temperatures [44]. As such, it may be beneficial to operate the MD system at lower temperatures to avoid scaling in the presence of these salts in the feed water. Figure 4 depicts the variation in optimum treatment cost for different MD inlet temperatures.

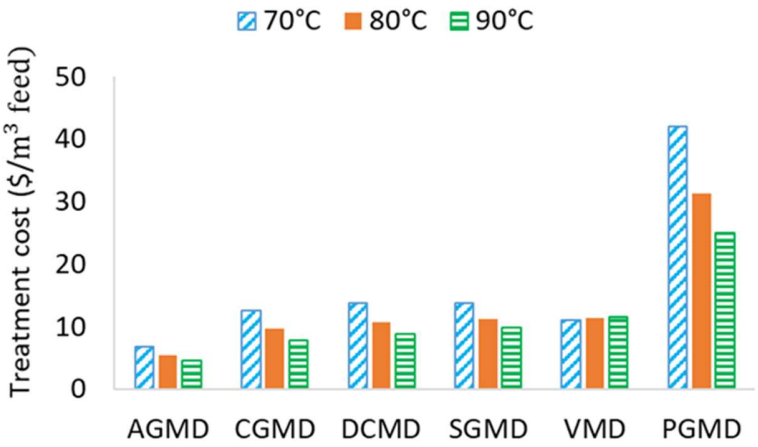

Figure 4. Variation in treatment cost as a function of MD inlet temperature

Except for VMD, lowering the MD inlet temperature increases the treatment cost for all MD configurations. This is because systems operating at higher MD inlet temperature generate higher fluxes initially along the module length, thereby increasing the average flux, thermal efficiency, and single pass recovery. Additionally, higher temperature enables the system to have higher heat recovery ratio and higher GOR.

Unlike other MD configurations, variations in MD inlet temperature has very little impact on the cost of VMD. This is consistent with the fact that the VMD configuration has minor heat recovery and its thermal efficiency does not vary significantly with temperature. Our analysis indicates that lowering the inlet temperature from 90 to 70°C results in a decrease in the optimum vacuum pressure from 17.3 kPa to 6.9 kPa, which enables high flux and avoiding large membrane area caused by low flux at lower inlet temperatures.

3.7.2 Brine salinity

Figure 5 shows the effect of brine salinity on the treatment cost and GOR for various MD configurations. At high recoveries, the salinity of the mixed stream (recycle stream and makeup feed) approaches that of the reject brine. As the reject brine salinity increases, the salinity and hence the vapor pressure lowering of the mixed stream in the hot channel increases. As a result, the systems' single pass recovery, thermal efficiency and energy recovery are reduced, resulting in lower GOR. Additionally, increase in the brine salinity while maintaining a constant make-up feed salinity increases the system's recovery ratio and required recycle ratio. As a result of the combined effect of a higher recycle ratio and a lower GOR, the treatment cost of the systems increases as the reject brine salinity rises. It should be noted that increasing the brine salinity has no discernible effect on the GOR for VMD, and the treatment cost decreases solely as a result of the change in recovery ratio. Figure 5 also illustrates that PGMD configuration is most sensitive to changes in reject brine salinity. As the brine salinity decreases from 30% to 20%, PGMD configuration outperforms VMD from a treatment cost point of view.

(a) (b)

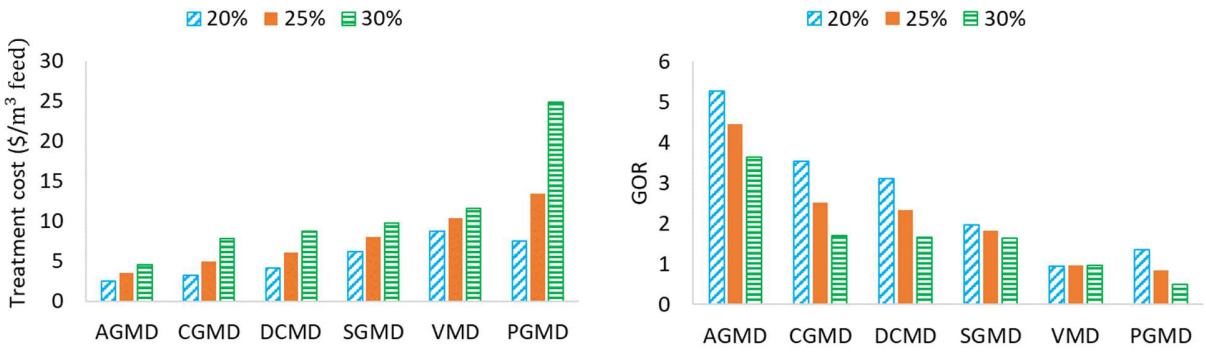

Figure 5. Optimal treatment cost and GOR as a function of reject brine salinity. The produced water salinity is fixed at 10%

3.7.3 Feed salinity

Figure 6 illustrates the effect of changes in produced water salinity on the optimal treatment cost of various MD configurations for a fixed reject brine salinity of 30%. As the feed salinity changes, the GOR and specific area of the systems remain unchanged. This is because the feed salinity has no impact on the operating salinity of the systems operating at high recoveries. As the system's feed salinity increases, both the recovery ratio and the required recycle ratio decrease. Thus, increasing the feed salinity reduces the system's treatment cost solely through the effect of decreasing the recycle ratio. Both Figures 5 and 6 demonstrate the critical effect of the recovery ratio in determining the magnitude of the difference between various MD configurations. As the recovery ratio increases (as a result of decreased feed salinity or increased reject brine salinity), the cost difference between various MD systems becomes more pronounced.

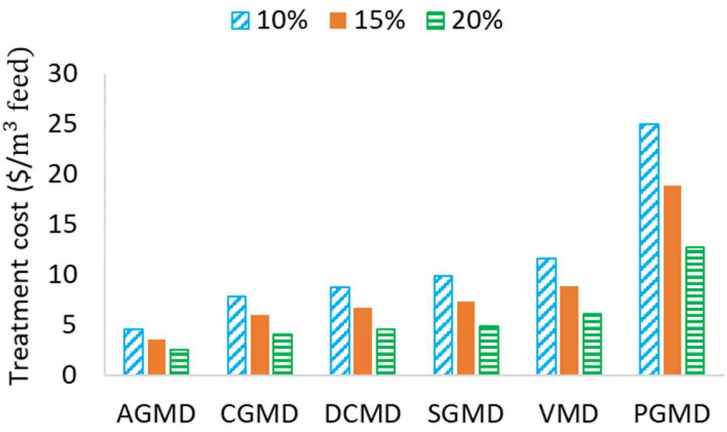

Figure 6. Effect of makeup feed salinity on optimal treatment cost

3.7.4 Gap width in PGMD and AGMD

In AGMD, operation at small gap sizes entails a risk of flooding in the air gap, reducing AGMD to PGMD mode of operation. As a result, larger gap sizes may be used to ensure successful performance of AGMD configuration. The available literature does not recommend a specific gap size as threshold for flooding because flooding is dependent on the condensation regime and permeate removal rate. In real systems, the common AGMD size is 1 mm [47]. However, several available studies show that gaps of 1mm or less are susceptible to flooding. [24, 47, 48]. As such, we establish a baseline gap size of 1mm for the ideal system and investigate the impact of increasing the gap size on the system's surface area, treatment cost, and GOR.

Figures 7a and b show that as the airgap size increases, both treatment cost and system area increase while the GOR decreases. This is because the mass flux resistance increases as the gap size increases, requiring the system with larger membrane area to achieve the same GOR as smaller gap sizes. Simultaneously, the high cost of the membrane prohibits using a very large

area. As a result of these two effects, increasing the gap size increases the membrane area but only to a limited extent, resulting in a net decrease in the GOR and an increase in total treatment cost. The gap analysis presented here is based on the assumption that there is no restriction on Re and that AGMD operates at its optimal low Re to maximize cost savings. When the effect of increasing gap and Re are combined, the impact on AGMD performance is even more detrimental. For instance, if AGMD must operate at Reynolds number of 1,500 and a large gap size of at least 3 mm, the cost of AGMD increases from \$4.57 to \$11.29/m^3feed, making it economically unattractive.

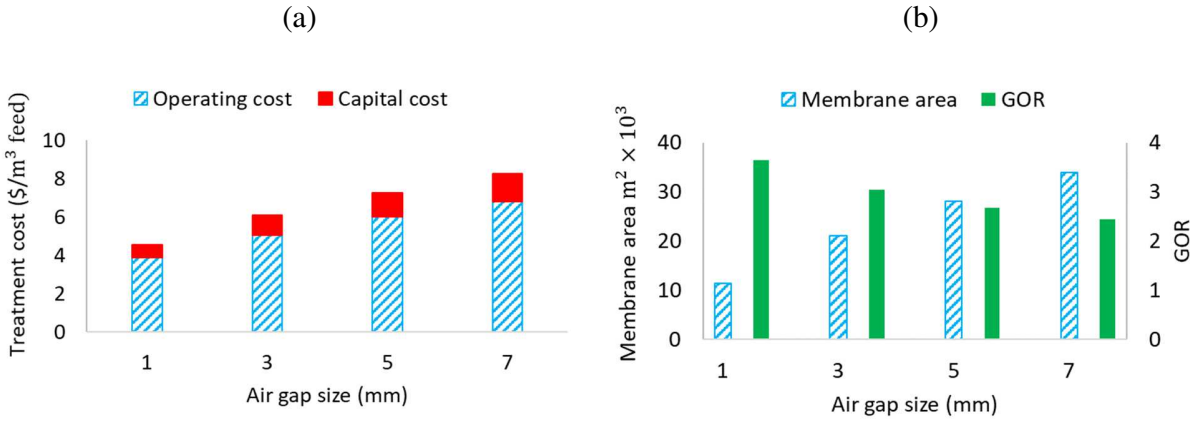

Figure 7. Effect of airgap size on a) optimal treatment cost b) membrane area and GOR of AGMD

PGMD configurations are not as prone to flooding as AGMD configurations and as such, no further analysis is provided for gap size larger than 1 mm. As previously described, the permeate gap in PGMD acts as an additional heat resistance layer that reduces the system's performance. As a result, the PGMD system needs to operate with smaller gap sizes to achieve better performance. However, operation at very small gaps may be prohibitive for successful performance of the system due to pressure buildup in the permeate gap, which prevents the

permeate from flowing out of the system [24]. As shown in Figure 8, smaller gap sizes result in lower treatment costs, smaller membrane area and higher GOR. This is because a smaller gap layer improves heat transfer, increasing both heat recovery and thermal efficiency, resulting in a higher GOR. Additionally, single pass recovery increases with smaller gap sizes, lowering the recycle ratio and requiring less total membrane area. It is worth noting that the gap size sensitivity analysis for CGMD is not performed because this configuration benefits from conductive material, which results in low gap heat resistance. As a result, unlike PGMD, CGMD does not necessitate a reduction in gap size to reduce the heat resistance of the gap.

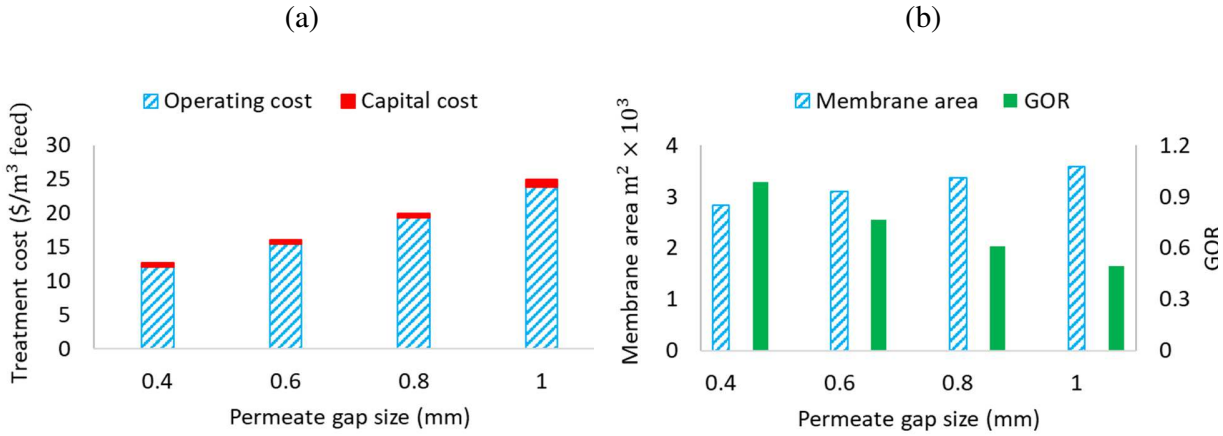

Figure 8. Effect of permeate gap size on a) treatment cost b) membrane area and GOR of PGMD

3.8 Membrane thickness in MD configurations

This analysis has shown that the GOR of PGMD, DCMD, and CGMD configurations is limited due to their relatively low thermal efficiency. Swaminathan et al. [24] highlighted the effect of increasing membrane thickness on enhancing GOR for CGMD system, assuming membranes as thick as 2 mm. Increasing the membrane thickness increases both conduction heat

resistance and mass transfer resistance, resulting in higher thermal efficiency and lower flux. In order to study the effect of membrane thickness on treatment cost, we use optimization models of DCMD, PGMD, and CGMD configurations with membrane thickness as the optimization variables. We then compare the optimum thickness that yields the lowest cost for each configuration with the results obtained using commercially available membranes (0.06 mm thickness).

(a)

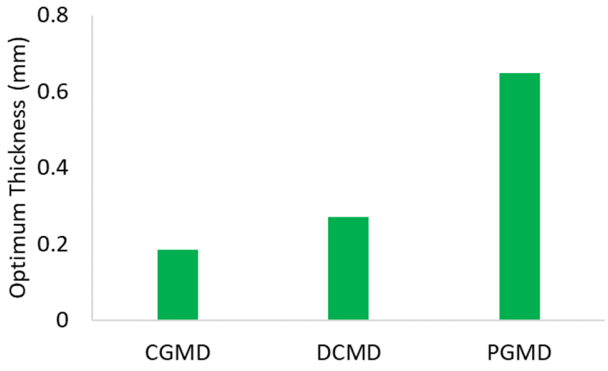

(b)

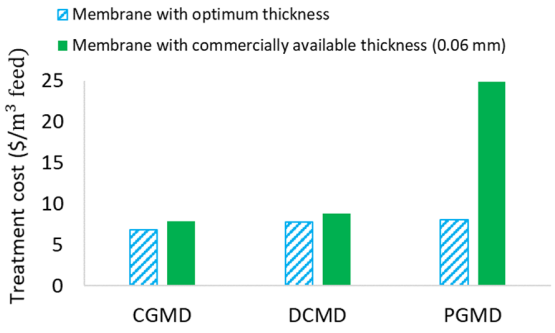

(c)

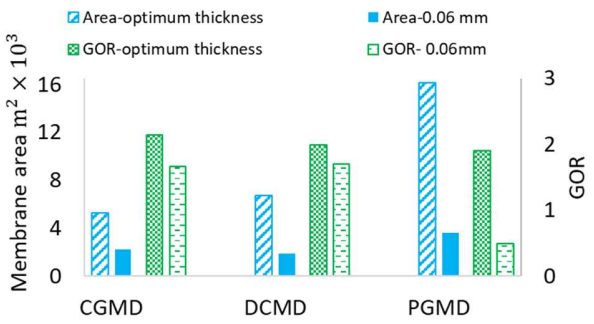

Figure 9. a) Optimum membrane thickness yielding minimum treatment cost, b) MD treatment cost at optimum membrane thickness and thickness of commercially available membranes (0.06 mm) c) Membrane area and GOR at optimum membrane thickness and thickness of commercially available membranes (0.06 mm)

Figure 9 shows optimum membrane thickness and a comparison of the treatment cost, membrane area, and GOR corresponding to optimum membrane thickness and actual membrane thickness of commercially available membrane (0.06mm thickness). All three configurations have optimum membrane thickness higher than 0.06 mm. These thicker membranes improve treatment cost and GOR in all configurations, but the membrane area increases because of reduced flux. To compensate for the negative effect of the permeate gap on thermal efficiency, PGMD requires a higher optimum thickness than DCMD and CGMD. PGMD also achieves the greatest cost savings and improvement in GOR as compared to DCMD and CGMD when operated using membranes with optimized thickness. This indicates that amongst all configurations, PGMD treatment cost shows the highest sensitivity to membrane thickness. When a sufficiently thick membrane is used, the GOR and cost performance of PGMD is comparable to that of CGMD and DCMD, but with a larger membrane area and lower flux.

The treatment cost of PGMD decrease to \$8.09/m^3_{feed} when optimum membrane thickness is used but a large membrane area of ~16,000 m^2 would be needed for a hypothetical treatment plant. This analysis is based on the constant permeate gap size of 1 mm. The combined effect of reducing the gap size (1 mm to 0.6 mm) and using the optimal membrane thickness results in the

treatment cost of \$8.06/m^3_{feed} for PGMD with a total membrane area of 8,995 m^2, which is comparable to the DCMD heat exchanger area but significantly less than that membrane area need in the AGMD system. In comparison to DCMD, CGMD has a lower optimum thickness because it can achieve high energy recovery and GOR with lower membrane thickness due to direct heat recovery within the module. Additionally, unit membrane cost for CGMD is higher than DCMD due to the additional cost of the conductive material. When operating at higher thickness and correspondingly large area, this results in a significant rise in CGMD cost due to the increased cost of the membrane, which counterbalances the benefit of increased thickness in terms of lowering the system's energy cost.

Cost-optimal design of each MD configuration requires consideration of numerous factors and theoretically cost-optimal design may not be the most attractive from a practical viewpoint. CGMD exhibits encouraging performance at reasonably high Reynolds numbers, resulting in a treatment cost of \$7.8/m^3_{feed} and membrane area of 2,250 m^2 which decreases to \$6.7/m^3_{feed} and membrane area of 5,260 m^2 using a membrane with optimal thickness. The optimal treatment cost for DCMD configuration is \$8.7/m^3_{feed} with a relatively high Reynolds number and a small membrane area of 2,000 m^2 but a large external heat exchanger of 8,000 m^2 The cost of DCMD drops to \$7.7/m^3_{feed} when a membrane of optimal thickness is used, while the membrane area increases to 6,000 m^2 and the external heat exchanger area decreases slightly to 7,500 m^2. Given the performance degradation of AGMD at high Re and large gaps, uncertainty in CGMD conductive material cost, the required membrane area (and hence system footprint), current availability of membranes with the desired thickness, and the process' practical success, DCMD appears to be the most attractive configuration from a practical viewpoint. With further

advancements in material types, thickness of MD membranes, and precise cost estimates for the conductive material, other MD configurations may have the potential to outperform DCMD.

4 Conclusions

We developed optimization models for the single stage continuous recirculation MD process for six MD configurations (DCMD, AGMD, PGMD, CGMD, VMD, and SGMD) with the objective of minimizing total unit cost of produced water treatment at ZLD condition. Stream properties (temperature, salinity, flowrate), membrane geometry, heat exchangers area, required energy (steam and electricity) are the optimization variables. We performed two series of optimization, one with membrane thickness set constant and the other with membrane thickness as one of the optimization variables. We compared the cost, membrane area, flux, specific area, GOR, thermal efficiency, heat recovery, single pass recovery, recycle ratio, and stream flow Reynolds number of the optimal design of the MD configuration. Additionally, we performed sensitivity analyses for the inlet temperature of the hot channel, feed salinity, brine salinity, and the gap size to study their effect on MD performance. The analysis was conducted for a hypothetical treatment plant with a capacity of 10 kg/s concentrating hypersaline produced water from 10% to 30% salinity. The following are the major findings from the study.

- For 1mm gap size and membrane with thin active layer of 0.06 mm, AGMD yields the lowest treatment cost of \$4.57/m^3_{feed}, followed by CGMD, DCMD, VMD, SGMD, and PGMD with treatment cost of 7.8, 8.7, 9.8, 11.63, and \$24.61/m^3_{feed}, respectively.
- Energy cost of heating and cooling constitute the major portion of the total treatment cost for all configurations. AGMD requires lowest energy with GOR of 3.6 and PGMD

requires the highest energy with GOR of 0.5. VMD, SGMD, and AGMD have the highest thermal efficiency, while AGMD, DCMD, and CGMD have the highest heat recovery.

- AGMD has the lowest flux of 2.1 LMH with the largest membrane area, while VMD and DCMD with the smallest membrane areas have the highest fluxes of 14.6 and 12.8 LMH, respectively.
- SGMD and AGMD operate at low Re of 50 and 317, respectively, to achieve the lowest cost, whereas all other configurations have Re greater than 1000. Increasing the Reynolds number of the SGMD and AGMD significantly increases their cost.
- All MD configurations have a low single pass recovery (up to 6.5 percent for AGMD) and a high recycle ratio. The highest single pass recovery and lowest recycle ratio are found in thermally efficient AGMD, SGMD, and VMD configurations.
- For all MD configurations, decreasing the MD inlet temperature increases the treatment cost (excluding VMD). The optimal vacuum pressure in VMD decreases as the inlet temperature decreases to maintain the high flux.
- When the brine salinity remains constant, increasing the feed salinity lowers the treatment cost because of the decrease in recycle ratio. The GOR of the system is independent of feed salinity at high recoveries. At high recoveries, the operating salinity of MD is highly dependent on brine salinity. Increasing brine salinity raises treatment costs due to a decrease in GOR and an increase in recycle ratio at constant feed salinity.
- In AGMD and PGMD, increasing the gap size increases membrane area while lowering GOR and treatment costs. PGMD may operate over smaller gap sizes, whereas AGMD requires larger gap sizes to avoid flooding. This reduces the difference in treatment costs

between these two configurations when comparing AGMD with larger air gap size than permeate gap size in PGMD.

- The optimum thickness of the membrane in DCMD, CGMD, and PGMD is greater than the constant thickness of 0.06 mm, with PGMD having the higher optimum thickness than the other two. By operating at their optimal thickness, the GOR and area of the configurations, particularly for PGMD, increase, while flux and treatment cost decrease.

Acknowledgement

This work was supported by the U.S. Department of Energy under Grant Number DE-EE0007888-10-08. Any findings expressed in this study are those of authors and do not reflect the views of the U.S. Department of Energy.

Nomenclature

Acronyms

AF	Amortization factor	
GOR	Gain output ratio	
CC	Capital cost	$\frac{\text{USD}}{\text{m}^3}$
OC	Operating cost	$\frac{\text{USD}}{\text{m}^3}$
LMTD	Log mean temperature difference	

Roman symbols

A	Area	m^2
B	Membrane Permeability	$\frac{\text{kg}}{\text{s.m}^2\text{.Pa}}$

B_0	Membrane Permeability coefficient	$\frac{kg}{s.m.Pa}$
C_p	Heat capacity.	$\frac{kJ}{kg.K}$
D	Solute diffusion coefficient	$\frac{m^2}{s}$
D_{ab}	Vapor diffusion coefficient into air	$\frac{m^2}{s}$
d_f	Spacer filament diamater	m
d_h	Membrane channel hydraulic diameter	m
h	enthalpy	$\frac{kJ}{kg}$
h_{conv}	Convection heat transfer coefficient	$\frac{kW}{K.m^2}$
J	flux	$\frac{kg}{s.m^2}$
k	Thermal conductivity	$\frac{kW}{K.m}$
k_{mass}	Mass transfer coefficient	$\frac{m}{s}$
L	Membrane length	m
M	Mass flow rate	$\frac{kg}{s}$
m	Molality	$\frac{mol}{kg}$
n	Molar flowrate	$\frac{mol}{s}$
Nu	Nusselt number	
P	Partial pressure	Pa

P_T	Total pressure	Pa
PD	Pressure drop	$\frac{Pa}{m}$
Pr	Prandtl number	
q	Heat flux	$\frac{kW}{m^2}$
R	Universal gas constant	$\frac{J}{mol.K}$
Re	Reynolds number	
Sc	Schmidt number	
Sh	Sherwood number	
T	Temperature	°C
U_{hx}	Overall heat transfer coefficient	$\frac{kW}{Km^2}$
V	Velocity	$\frac{m}{s}$
W	Membrane width	m
X	Salinity (weight percent)	%

Greek symbols

ρ	density	$\frac{kg}{m^3}$
μ	viscosity	Pa.s
ΔT	Temperature difference	°C
ΔA	Slice area	m^2
α	Activity coefficient	

δ	thickness	m
θ	Terminal temperature differences in heat exchangers	°C
η	Energy efficiency	%
ϵ	porosity	%

subscripts

a	Air side
ave	average
b	Bulk
c	Cold side
ch	chiller
cond	conduction
conv	convection
cw	Cooling wall
e	evaporation
f	Make up feed
ff	Falling film
g	gap
h	Hot side
hx	Heat exchanger
in	inlet
l	Liquid
m	Membrane surface
Mix	Mixture of makeup feed and recycle stream

out	outlet
p	Permeate
rec	Recycle stream
sat	saturation
sl	Saturated liquid
sp	spacer
sv	Saturated vapor
v	vapor
vac	Vacuum side

superscripts

z	Slice number
firstz	First slice
lastz	Last slice

References

1. Krishna, H.J., *Introduction to desalination technologies.* Texas water development, 2004. **2**.
2. Shaffer, D.L., et al., *Desalination and reuse of high-salinity shale gas produced water: drivers, technologies, and future directions.* Environmental science & technology, 2013. **47**(17): p. 9569-9583.
3. Kaplan, R., et al., *Assessment of desalination technologies for treatment of a highly saline brine from a potential CO2 storage site.* Desalination, 2017. **404**: p. 87-101.
4. Singh, R., *Membrane technology and engineering for water purification: application, systems design and operation*. 2014: Butterworth-Heinemann.

5. Barbot, E., et al., *Spatial and temporal correlation of water quality parameters of produced waters from Devonian-age shale following hydraulic fracturing.* Environmental science & technology, 2013. **47**(6): p. 2562-2569.
6. Kondash, A.J., E. Albright, and A. Vengosh, *Quantity of flowback and produced waters from unconventional oil and gas exploration.* Science of the Total Environment, 2017. **574**: p. 314-321.
7. Pichtel, J., *Oil and gas production wastewater: Soil contamination and pollution prevention.* Applied and Environmental Soil Science, 2016. **2016**.
8. Olmstead, S.M., et al., *Shale gas development impacts on surface water quality in Pennsylvania.* Proceedings of the National Academy of Sciences, 2013. **110**(13): p. 4962-4967.
9. Brittingham, M.C., et al., *Ecological risks of shale oil and gas development to wildlife, aquatic resources and their habitats.* Environmental science & technology, 2014. **48**(19): p. 11034-11047.
10. Clark, C.E. and J.A. Veil, *Produced water volumes and management practices in the United States*. 2009, Argonne National Lab.(ANL), Argonne, IL (United States).
11. Lutz, B.D., A.N. Lewis, and M.W. Doyle, *Generation, transport, and disposal of wastewater associated with Marcellus Shale gas development.* Water Resources Research, 2013. **49**(2): p. 647-656.
12. Ellsworth, W.L., *Injection-induced earthquakes.* Science, 2013. **341**(6142).
13. Horton, S., *Disposal of hydrofracking waste fluid by injection into subsurface aquifers triggers earthquake swarm in central Arkansas with potential for damaging earthquake.* Seismological Research Letters, 2012. **83**(2): p. 250-260.
14. Keranen, K.M., et al., *Sharp increase in central Oklahoma seismicity since 2008 induced by massive wastewater injection.* Science, 2014. **345**(6195): p. 448-451.
15. Basile, A. and C. Charcosset, *Integrated membrane systems and processes*. 2016: Wiley Online Library.
16. Tavakkoli, S., et al., *Shale gas produced water management using membrane distillation: An optimization-based approach.* Resources, Conservation and Recycling, 2020. **158**: p. 104803.
17. Lokare, O.R., et al., *Importance of feed recirculation for the overall energy consumption in membrane distillation systems.* Desalination, 2018. **428**: p. 250-254.
18. Swaminathan, J., *Design and operation of membrane distillation with feed recirculation for high recovery brine concentration.* Desalination, 2018. **445**: p. 51-62.
19. He, F., J. Gilron, and K.K. Sirkar, *High water recovery in direct contact membrane distillation using a series of cascades.* Desalination, 2013. **323**: p. 48-54.
20. Alkhudhiri, A., N. Darwish, and N. Hilal, *Membrane distillation: a comprehensive review.* Desalination, 2012. **287**: p. 2-18.
21. Swaminathan, J., et al., *Energy efficiency of permeate gap and novel conductive gap membrane distillation.* Journal of Membrane Science, 2016. **502**: p. 171-178.
22. Drioli, E., A. Ali, and F. Macedonio, *Membrane distillation: Recent developments and perspectives.* Desalination, 2015. **356**: p. 56-84.
23. Summers, E.K. and H.A. Arafat, *Energy efficiency comparison of single-stage membrane distillation (MD) desalination cycles in different configurations.* Desalination, 2012. **290**: p. 54-66.
24. Swaminathan, J., H.W. Chung, and D.M. Warsinger, *Energy efficiency of membrane distillation up to high salinity: Evaluating critical system size and optimal membrane thickness.* Applied Energy, 2018. **211**: p. 715-734.
25. El Amali, A., S. Bouguecha, and M. Maalej, *Experimental study of air gap and direct contact membrane distillation configurations: application to geothermal and seawater desalination.* Desalination, 2004. **168**: p. 357.

26. Alklaibi, A.M. and N. Lior, *Comparative study of direct-contact and air-gap membrane distillation processes.* Industrial & engineering chemistry research, 2007. **46**(2): p. 584-590.
27. Eykens, L., et al., *How to select a membrane distillation configuration? Process conditions and membrane influence unraveled.* Desalination, 2016. **399**: p. 105-115.
28. Khalifa, A.E., *Water and air gap membrane distillation for water desalination–an experimental comparative study.* Separation and Purification Technology, 2015. **141**: p. 276-284.
29. Cheng, L., et al., *Comparative study of air gap and permeate gap membrane distillation using internal heat recovery hollow fiber membrane module.* Desalination, 2018. **426**: p. 42-49.
30. Noamani, S., et al., *Modeling of Air-Gap Membrane Distillation and Comparative Study with Direct Contact Membrane Distillation.* Industrial & Engineering Chemistry Research, 2020. **59**(50): p. 21930-21947.
31. Kesieme, U.K., et al., *Economic analysis of desalination technologies in the context of carbon pricing, and opportunities for membrane distillation.* Desalination, 2013. **323**: p. 66-74.
32. Al-Obaidani, S., et al., *Potential of membrane distillation in seawater desalination: thermal efficiency, sensitivity study and cost estimation.* Journal of Membrane Science, 2008. **323**(1): p. 85-98.
33. Sirkar, K.K. and L. Song, *Pilot-scale studies for direct contact membrane distillation-based desalination process*. 2009: US Department of the Interior, Bureau of Reclamation.
34. Schwantes, R., et al., *Techno-economic comparison of membrane distillation and MVC in a zero liquid discharge application.* Desalination, 2018. **428**: p. 50-68.
35. Hitsov, I., et al., *Economic modelling and model-based process optimization of membrane distillation.* Desalination, 2018. **436**: p. 125-143.
36. Tavakkoli, S., et al., *A techno-economic assessment of membrane distillation for treatment of Marcellus shale produced water.* Desalination, 2017. **416**: p. 24-34.
37. Carrero-Parreño, A., et al., *Optimization of multistage membrane distillation system for treating shale gas produced water.* Desalination, 2019. **460**: p. 15-27.
38. Bartholomew, T.V., et al., *Cost optimization of high recovery single stage gap membrane distillation.* Journal of Membrane Science, 2020. **611**: p. 118370.
39. Lokare, O.R., et al., *Integrating membrane distillation with waste heat from natural gas compressor stations for produced water treatment in Pennsylvania.* Desalination, 2017. **413**: p. 144-153.
40. Drud, A.S., *CONOPT—a large-scale GRG code.* ORSA Journal on computing, 1994. **6**(2): p. 207-216.
41. Sievers, M. and J.H. Lienhard, *Design of flat-plate dehumidifiers for humidification–dehumidification desalination systems.* Heat transfer engineering, 2013. **34**(7): p. 543-561.
42. Swaminathan, J., *Numerical and experimental investigation of membrane distillation flux and energy efficiency*. 2014, Massachusetts Institute of Technology.
43. Lin, S., N.Y. Yip, and M. Elimelech, *Direct contact membrane distillation with heat recovery: Thermodynamic insights from module scale modeling.* Journal of membrane science, 2014. **453**: p. 498-515.
44. Warsinger, D.M., et al., *Scaling and fouling in membrane distillation for desalination applications: a review.* Desalination, 2015. **356**: p. 294-313.
45. Guan, G., et al., *Achieving sustainable operation for hypersaline membrane distillation applications: A novel strategy based on the critical Reynolds number.* Desalination, 2021. **499**: p. 114833.
46. Warsinger, D.M., E.W. Tow, and J. Swaminathan, *Theoretical framework for predicting inorganic fouling in membrane distillation and experimental validation with calcium sulfate.* Journal of Membrane Science, 2017. **528**: p. 381-390.

47. Warsinger, D.M., J. Swaminathan, and L.L. Morales, *Comprehensive condensation flow regimes in air gap membrane distillation: Visualization and energy efficiency.* Journal of membrane science, 2018. **555**: p. 517-528.
48. Hitsov, I., et al., *Full-scale validated Air Gap Membrane Distillation (AGMD) model without calibration parameters.* Journal of membrane science, 2017. **533**: p. 309-320.
49. Towler, G. and R. Sinnott, *Chemical engineering design: principles, practice and economics of plant and process design*. 2012: Elsevier.
50. Karanikola, V., et al., *Economic performance of membrane distillation configurations in optimal solar thermal desalination systems.* Desalination, 2019. **472**: p. 114164.
51. Alsaadi, A.S., et al., *Modeling of air-gap membrane distillation process: A theoretical and experimental study.* Journal of membrane science, 2013. **445**: p. 53-65.
52. Karanikola, V., et al., *Sweeping gas membrane distillation: numerical simulation of mass and heat transfer in a hollow fiber membrane module.* Journal of Membrane Science, 2015. **483**: p. 15-24.
53. Chung, H.W., J. Swaminathan, and D.M. Warsinger, *Multistage vacuum membrane distillation (MSVMD) systems for high salinity applications.* Journal of Membrane Science, 2016. **497**: p. 128-141.
54. Lee, J.-G., et al., *Performance modeling of direct contact membrane distillation (DCMD) seawater desalination process using a commercial composite membrane.* Journal of Membrane Science, 2015. **478**: p. 85-95.
55. Gryta, M., M. Tomaszewska, and A. Morawski, *Membrane distillation with laminar flow.* Separation and Purification Technology, 1997. **11**(2): p. 93-101.
56. García-Payo, M.d.C. and M.A. Izquierdo-Gil, *Thermal resistance technique for measuring the thermal conductivity of thin microporous membranes.* Journal of Physics D: Applied Physics, 2004. **37**(21): p. 3008.
57. Hitsov, I., et al., *Modelling approaches in membrane distillation: A critical review.* Separation and Purification Technology, 2015. **142**: p. 48-64.
58. Da Costa, A., A. Fane, and D. Wiley, *Spacer characterization and pressure drop modelling in spacer-filled channels for ultrafiltration.* Journal of membrane science, 1994. **87**(1-2): p. 79-98.
59. Winter, D., *Membrane distillation: A thermodynamic, technological and economic analysis*. 2015: Shaker Verlag.
60. Guillen, G. and E.M. Hoek, *Modeling the impacts of feed spacer geometry on reverse osmosis and nanofiltration processes.* Chemical Engineering Journal, 2009. **149**(1-3): p. 221-231.
61. El-Dessouky, H.T. and H.M. Ettouney, *Fundamentals of salt water desalination*. 2002: Elsevier.

Appendix

The data and parameters used in the modeling process are listed in Tables A.1 to A.4.

Table A.1. Plant characteristics and annual cost estimation (baseline values)

Produced water temperature (°C)	2

Produced water salinity (%)	10
Reject brine salinity (%)	30
Plant capacity (kg/s)	10
Steam temperature	140
Maximum stream temperature (°C)	90
Minimum stream temperature (°C)	10
Maximum stream salinity (%)	30
Plant life (year)	20
Interest rate (5)	5

Table A.2. Membrane properties (baseline values)

Membrane type	PTFE with PP support	Ref
Membrane permeability coefficient* $\left(\frac{\text{kg}}{\text{s.m.Pa}}\right)$	0.936×10^{-10}	[39]
Membrane thermal conductivity $\left(\frac{\text{kW}}{\text{m.K}}\right)$	0.000242	[39]
Overall thickness of the membrane	148 µm	[39]

Active layer thickness (μm)	60	[39]
Membrane porosity (%)	60	[39]
Support thermal conductivity $\left(\frac{kW}{m.K}\right)$	0.00023	[39]
Air thermal conductivity $\left(\frac{kW}{m.K}\right)$	0.000024	
Conductive gap thermal conductivity $\left(\frac{kW}{m.K}\right)$	0.01	[21]
Permeate gap thermal conductivity $\left(\frac{kW}{m.K}\right)$	0.00006	[21]
Gap size (mm)	1	
Air gap spacer thermal conductivity $\left(\frac{kW}{m.K}\right)$	0.0002	[24]
Condensing surface thickness (mm)	1.5	
Cooling wall thermal conductivity $\left(\frac{kW}{m.K}\right)$	0.06	
Spacer porosity	77%	[39]
Spacer thickness	1.9 mm	[39]
Filament diameter	1.2 mm	[39]
Overall heat transfer coefficient (liquid-liquid heat exchangers)	1.3 $\frac{kW}{m^2.K}$	Assumed
Overall heat transfer coefficient (liquid-condensing vapor heat exchangers)	2 $\frac{kW}{m^2.K}$	Assumed

*calculated using the production of the active layer thickness and membrane permeability ($B_0 = B \times \delta_m$) obtained from ref [39].

Table A.3. Capital cost data (baseline values)

Capital Cost	Base price	Base capacity	Scale up	Ref.

			coefficient	
Membrane (AGMD, PGMD, CGMD)	90 ($\frac{\$}{m^2}$)			[35]
Membrane (DCMD, VMD, SGMD)	56 ($\frac{\$}{m^2}$)			[35]
Membrane Module (AGMD, PGMD, CGMD)	2340 ($\frac{\$}{module}$)	3 modules	0.8	[35]
Membrane module (DCMD, VMD, SGMD)	1080 ($\frac{\$}{module}$)	3 modules	0.8	[35]
CGMD conductive material*	390 ($\frac{\$}{m^2}$)			assumed
Feed water storage Tanks	0.5 ($\frac{\$}{gal}$)			[36]
Permeate water storage Tanks	0.4 ($\frac{\$}{gal}$)			[36]
Heating and cooling installation each	5	10 ($\frac{m^3}{h}$)	0.6	[35]
Heat exchanger	390 ($\frac{\$}{m^2}$)			[35]
Heat exchanger endplate	950($\frac{\$}{module}$)			[35]
Chiller	200 ($\frac{\$}{kWh}$)			[38]
Pump	9052.35 ($\frac{\$}{unit}$)			[49]
Pump	271.57 ($\frac{\$}{liter/s}$)	1 ($\frac{liter}{s}$)	0.9	[49]
Blower	675.36	1 kW	0.5135	[50]

* For CGMD membrane, the gap conductivity is increased by filling the gap with conductive material such as metal mesh, metal foam, or using finned condenser surface. [21]. We assumed the specially designed finned copper surface in reference [21] with thermal conductivity of 10 $\frac{W}{m.K}$ is used in CGMD. This process incure additional cost per square meter of membrane area to the system. Since this CGMD is developed in the lab scale we don't have any

data about the amount and total cost of the material used to obtain thermal conductivity of in the gap. Therefore, for the purpose of this study, we assumed the same price used for heat exchanger to be applicable to the conductive material filling per unit of area.

Table A.4. Operating cost data (baseline values)

Operating cost		Ref.
Steam	0.008 $\left(\frac{\$}{kg}\right)$	[36]
Electricity	0.069$\left(\frac{\$}{kwh}\right)$	[36]
Membrane replacement	Every four years	Assumed
Pretreatment cost	0.058 $\left(\frac{\$}{\text{kg feed}}\right)$	[35]

Methodology

Our modeling closely follows the approaches described in references [21, 23, 42, 48, 51-53], as summarized in tables A.5. and A.6, followed by correlations in table A.7.

It is worth noting that we assume that only the active layer contributes to mass transfer, as demonstrated in [54], and that the support layer has a negative impact on heat transfer, as described in [55].

Table A.5. Heat balance equations for MD systems

Heat flux for $z \in Z$					
	DCMD	AGMD	PGMD/CGMD	SGMD	VMD
Convective heat -hot channel	$q^z_{conv_h} = h^z_h\left(T^z_{h_b} - T^z_{h_m}\right)$				

Convective heat -cold channel	$q^z_{conv_c} = h^z_h\left(T^z_{c_m} - T^z_{c_b}\right)$				-
Conductive heat-membrane	$q^z_{cond_m} = \frac{k_m}{\delta_m}\left(T^z_{h_m} - T^z_{c_m}\right)$	$q^z_{cond_m} = \frac{k_m}{\delta_m}\left(T^z_{h_m} - T^z_{g_m}\right)$		$q^z_{cond_m} = \frac{k_m}{\delta_m}\left(T^z_{h_m} - T^z_{a_m}\right)$	-
Conductive heat-gap	-	$q^z_{cond_g} = \frac{k_g}{\delta_g - \delta_{ff}}\left(T^z_{g_m} - T^z_{ff}\right)$	$q^z_{cond_g} = \frac{k_g}{\delta_g}\left(T^z_{g_m} - T^z_{cw}\right)$	-	-
Conductive heat-falling film		$q^z_{cond_{ff}} = \frac{k_w}{\delta_{ff}}\left(T^z_{ff} - T^z_{cw}\right)$			
Vapor expansion heat	-	-	-	-	$q^z_{exp} = RT^z_{h_m}\log\left(\frac{P_{h_m}}{P_{vac}}\right)$
Heat of evaporation/ condensation	$q^z_e(T) = J^z H^z_e(T)$				
Heat of condensation in air channel	-				$q^z_c(T) = Jc^z H^z_e(T)$
Heat balances for $z \in Z$					
	DCMD	AGMD	PGMD/CGMD	SGMD	VMD
Heat balace1	$q^z_{conv_h} = q^z_{cond_m} + q^z_e\left(T^z_{h_m}\right) + C^z_p\left(T^z_{h_m} - T^z_{h_b}\right)$				$q^z_{conv_h} = q^z_{exp} + q^z_e\left(T^z_{h_m}\right) + C^z_p\left(T^z_{h_m} - T^z_{h_b}\right)$
Heat balance2	$q^z_{conv_c} = q^z_{cond_m} + q^z_e\left(T^z_{c_m}\right) + C^z_p\left(T^z_{c_m} - T^z_{c_b}\right)$	$q^z_{conv_c} = q^z_{cond_{ff}} + C^z_p\left(T^z_{ff} - T^z_{cp}\right)$	$q^z_{conv_c} = q^z_{cond_m} + q^z_e\left(T^z_{g_m}\right)$	$q^z_{conv_a} = q^z_{cond_m} + C^z_{pv}\left(T^z_{h_m} - T^z_{a_b}\right)$	-

Heat balance 3	-	$q^z_{cond_m} = q^z_{cond_g}$	$q^z_{cond_m} + q^z_e(T^z_{g_m}) = q^z_{cond_g}$	-	-
Heat balance 4		$q^z_{cond_{ff}} = \frac{k_w}{\delta_{ff}}(T^z_{ff} - T^z_{cp})$			
Enthalpy balance for $z \in Z$					
	DCMD	AGMD	PGMD/CGMD	SGMD	VMD
Enthalpy balance-hot channel	$q^z_{conv_h} L^z W = M^z_{h_{in}} C^z_p (T^z_{h_{in}} - T^z_{h_{out}})$				
Enthalpy balance-cold channel	$q^z_{conv_c} L^z W = M^z_{c_{in}} C^z_p (T^z_{c_{out}} - T^z_{c_{in}})$			$q^z_{conv_c} L^z W + q^z_c(T^z_{a_b}) = (M^z_{a_{in}} C^z_{pa} + m^z_{v_{in}} C^z_{pv}) \times (T^z_{a_{out}} - T^z_{a_{in}})$	-
Enthalpy balance-heater	$M_s h_{v_s} = (M_f + M_{rec}) C_p (T_{chx_{out}} - T^z_{h_{in}})$, Z=1				$M_s h_{v_s} = (M_f + M_{rec}) C_p (T_{mix} - T^z_{h_{in}})$, Z=1
Enthalpy balance-external heat exchanger/ condenser	$(M_f + M_{rec}) C_p (T_{chx_{out}} - T_{mix}) = M^z_{c_{in}} C_p (T_{h_{hx_{in}}} - T_{h_{hx_{out}}})$ $z = lastz$	-	-	$(M_f + M_{rec}) C_p (T_{chx_{out}} - T_{mix}) = M^z_{a_{in}} (T^{firstz}_{a_{out}} - T^{lastz}_{a_{in}}) + M_{p_{tot}} h_v(T_{sat})$	$(M_f + M_{coolant}) C_p (T_{chx_{out}} - T_{mix}) = M_{p_{tot}} h_v(T_{sat_{vac}})$
Chiller energy demand	$Q_{ch} = M^z_{c_{in}} C_p (T_{h_{hx_{in}}} - T_{ch_{out}})/COP$ $z = lastz$	$Q_{ch} = M_{rec} C_p (T^z_{h_{out}} - T_{ch_{out}})/COP$ $z = lastz$			$Q_{ch} = M_{coolant} C_p (T_{ch_{in}} - T_{ch_{out}})/COP$
Heat transfer area	$A_{hx,cond,heater} = \frac{Q_{hx} LMTD}{U_{hx}}$				

Table A.6. Mass balance equations and correlations for MD systems

Mass balance					
	DCMD	AGMD	PGMD/CGMD	SGMD	VMD
Hot channel	$M^z_{h_{in}} = M_{rec} + M_f \quad z = 1$ $M^z_{h_{out}} = M^z_{h_{in}} - M^z_p \quad z \in Z$ $M^j_{h_{out}} = M_{rec} + M_{rej} \quad z = lastz$ $M^z_{h_{out}} X^z_{h_{out}} = M^z_{h_{in}} X^z_{h_{out}} \quad z \in Z$				
Cold channel $z \in Z$	$M^z_{c_{in}} + M^z_p = M^z_{c_{out}}$	$M^z_{c_{in}} = M^z_{c_{out}} = M^z_{h_{in}} = M_{rec} + M_f$		$M^z_{a_{in}} = M^z_{a_{out}}$ $M^z_{v_{in}} + M^z_p$ $= M^z_{v_{out}} + M^z_p$	$M^z_{v_{in}} + M^z_p$ $= M^z_{v_{out}}$
Permeate mass $z \in Z$	$M^z_p = J^z L^z W$ $M_{p_{tot}} = \sum_z M^z_p$				
Mass flux					
	DCMD	AGMD	PGMD/CGMD	SGMD	VMD
Permeate flux	$J^z = B\left(P^z_{sat_{h_m}} - P^z_{sat_{h_c}}\right)$	$J^z = B\left(P^z_{sat_{h_m}} - P^z_{sat_{ff}}\right)$	$J^z = B\left(P^z_{sat_{h_m}} - P^z_{sat_{g_m}}\right)$	$J^z = B\left(P^z_{sat_{h_m}} - P^z_{a_b}\right)$	$J^z = B\left(P^z_{sat_{h_m}} - P^z_{vac}\right)$
Air channel partial vapor pressure	-	-	-	$P_{a_b} = \frac{n_v}{n_a + n_v} P_T$ $: P_{a_b} \le P_{sat_{a_b}}$	-
Saturation pressure	$P_{sat} = \alpha \times \exp\left(23.5377 - \frac{4016.3632}{T + 273.15 - 38.6339}\right)$				
Permeability coefficient	$B = \frac{B_0}{\delta_m}$	$B = \left(\frac{\delta_m}{B_0} + \frac{\delta_g - \delta_{ff}}{B_a}\right)^{-1}$	$B = \frac{B_0}{\delta_m}$	$B = \left(\frac{\delta_m}{B_0} + \frac{d_{h_a}}{B_a sh}\right)^{-1}$	$B = \frac{B_0}{\delta_m}$
air gap/channel	-	$B_a = \frac{D_{ab} M_w}{R T_{ave}}$		-	-

permeability coefficient				
Diffusion coefficient	-	$D_{ab} = \frac{1.895 \times 10^{-5} \times T_{ave}^{2.072}}{P_T}$	-	-
Falling film thickness		$J^z = \frac{\rho_l(\rho_l - \rho_v)g\delta_f^2}{\mu}\frac{d\delta_f}{dz}$		
Concentration polarization	$X_m^z = X_b^z \exp\left(\frac{J^z}{k_{mass}\rho}\right)$			

Table A.7. Correlations

Brine heat capacity	$C_p = 15.556m^2 - 241.78m + 4116.9$	[18]
Brine viscosity	$\mu = 2.239 \times 10^{-4} m^{0.2306}$	[18]
Brine density	$\rho = 1028.58 + 38.23m - 1.043m^2$	[18]
Brine thermal conductivity	$K = 0.6465 - 00581 \times 10^{-3}m - 0.000154 \times 10^{-4}m^2$	[18]
Effective thermal conductivity of a porous medium	$k_{eff} = \frac{k_{gas}(1 + 2\beta(1-\epsilon))}{1 - \beta(1-\epsilon)}$ $\beta = \left(k_{solid} - k_{gas}\right) / \left(k_{solid} + 2k_{gas}\right)$	[56]
Brine activity coefficient	$\alpha = 1 - 0.03112m - 0.001482m^2$	[57]
Hydraulic diameter	$d_h = \frac{4\varepsilon d_f \delta_{sp}}{\left(2d_f + 4(1-\varepsilon)\delta_{sp}\right)}$	[58]

Velocity	$V = \frac{M_{in}}{(W_m \delta_{sp} \varepsilon \rho)}$	
Reynolds number	$Re = \frac{\rho V d_h}{\mu}$	
Prandtl's number	$Pr = \frac{\mu C_p}{k}$	
Schmidt number	$Sc = \frac{\mu}{\rho . D}$	
Sherwood number	$Sh = 0.162 Re^{0.656} Sc^{0.333}$	
Membrane Nusselt number	$Nu = 0.162 Re^{0.656} Pr^{0.333}$	[59]
Condenser Nusselt number	$Nu = 0.37 Re^{0.67} Pr^{0.33}$	[50]
Mass transfer coefficient	$k_{mass} = \frac{D . Sh}{d_h}$	
Pressure drop	$PD = \left(0.42 + \frac{189.3}{Re}\right) \frac{\rho V^2}{2 d_h}$	[60]
Enthalpy of evaporation	$H_e = 2501.897149 - 2.407064037\, T + 1.92217 \times 10^{-3} T - 1.5863 \times 10^{-5} T$	[61]
Saturated water enthalpy	$H_{sl} = -0.033635409 + 4.20557011\, T - 6.200339 \times 10^{-4} T^2 + 4.459374 \times 10^{-6} T^3$	[61]

Table A.8. Detailed treatment cost split for various MD configurations ($/m$^3_{feed}$)

	AGMD	DCMD	CGMD	PGMD	SGMD	VMD

Capital costs	Chiller	0.03	0.08	0.08	0.28	0.08	0.13
	Heat exchangers	0.01	0.91	0.011	0.03	1.33	0.05
	Membrane and modules	0.38	0.06	0.279	0.14	0.17	0.04
	Installations (pumps and pipes)	0.09	0.11	0.08	0.101	0.07	0.04
	Blower	-	-	-	-	0.01	-
	Vacuum pump	-	-	-	-	-	0.01
Operating costs	Chilling	1.16	2.79	2.64	9.48	2.59	4.33
	Heating	1.77	3.87	3.81	13.13	3.94	6.59
	Membrane replacement	0.85	0.14	0.25	0.31	0.38	0.09
	Pump	0.08	0.5	0.51	0.93	0.04	0.03
	Blower	-	-	-	-	1.05	-
	Vacuum pump	-	-	-	-	-	0.01
	Others	0.08	0.08	0.08	0.08	0.08	0.08

Table A.9. Performance metrics and operating conditions for various MD configurations at their cost optimal design

	AGMD	CGMD	DCMD	SGMD	VMD	PGMD
Unit treatment cost ($/m$^3_{feed}$)	4.57	7.86	8.77	9.81	11.56	24.61
Unit operating cost ($/m$^3_{feed}$)	3.86	7.16	7.30	7.96	11.11	23.86
Unit capital cost ($/m$^3_{feed}$)	0.71	0.70	1.47	1.85	0.46	1.06
Total membrane area (m^2)	11.30	2.26	1.88	8.14	1.72	3.58
Specific membrane area $\left(m^2/kg\right)$	110.71	12.05	10.93	63.44	8.74	11.51
Flux (LMH)	2.13	10.81	12.84	2.96	14.06	6.73
GOR	3.64	1.70	1.67	1.65	1.07	0.49
Electricity consumption (pumps and chilling) (kWh/m^3_{feed})	17.97	45.65	50.29	53.33	63.33	150.87
Thermal efficiency (%)	74.50	42.90	45.70	98.20	96.80	35.70
Heat recovery (%)	83.00	79.80	72.20	61.90	0.00	58.00
Single pass recovery (%)	6.50	3.60	3.90	5.20	4.60	2.10
Recycle ratio $\left(kg/kg\right)$	9.21	17.59	16.19	11.83	13.41	30.11
Reynolds number	317.3	1225.7	1432.4	50	1040.3	1288
Hot channel inlet temperature (℃)	90	90	90	90	90	90
Hot channel outlet temperature (℃)	24.27	26.17	25.30	49.17	73.14	43.95

Cold channel inlet temperature (℃)	11.91	10.61	10	33.6	64.7	10.36
Cold channel outlet temperature (℃)	76.04	73.49	73.94	80.62	64.7	56.1

Sensitivity analysis- costs elements: Figure A1 depicts the variation in optimum treatment costs as a function of the cost elements (including cost of steam, electricity, membrane and module replacement, and membrane replacement) as compared to the baseline value (BV) of the costs considered in this study's main analysis. The current sensitivity analysis is performed by multiplying the baseline value of the above-mentioned costs by 50% and 150%. Regardless of changes in BV of cost elements, the order of superiority of performance of various MD configurations remains constant, with AGMD outperforming all other configurations. Reducing the unit cost of steam and electricity has a significant effect on lowering the treatment cost of all MD configurations (figure A1a and A1b), as heating and chilling costs account for the majority of MD system treatment costs. Except for AGMD with large membrane areas, changes in the membrane and module and membrane replacement cost have no significant effect on MD treatment costs (figure A1c and A1d).

a) b)

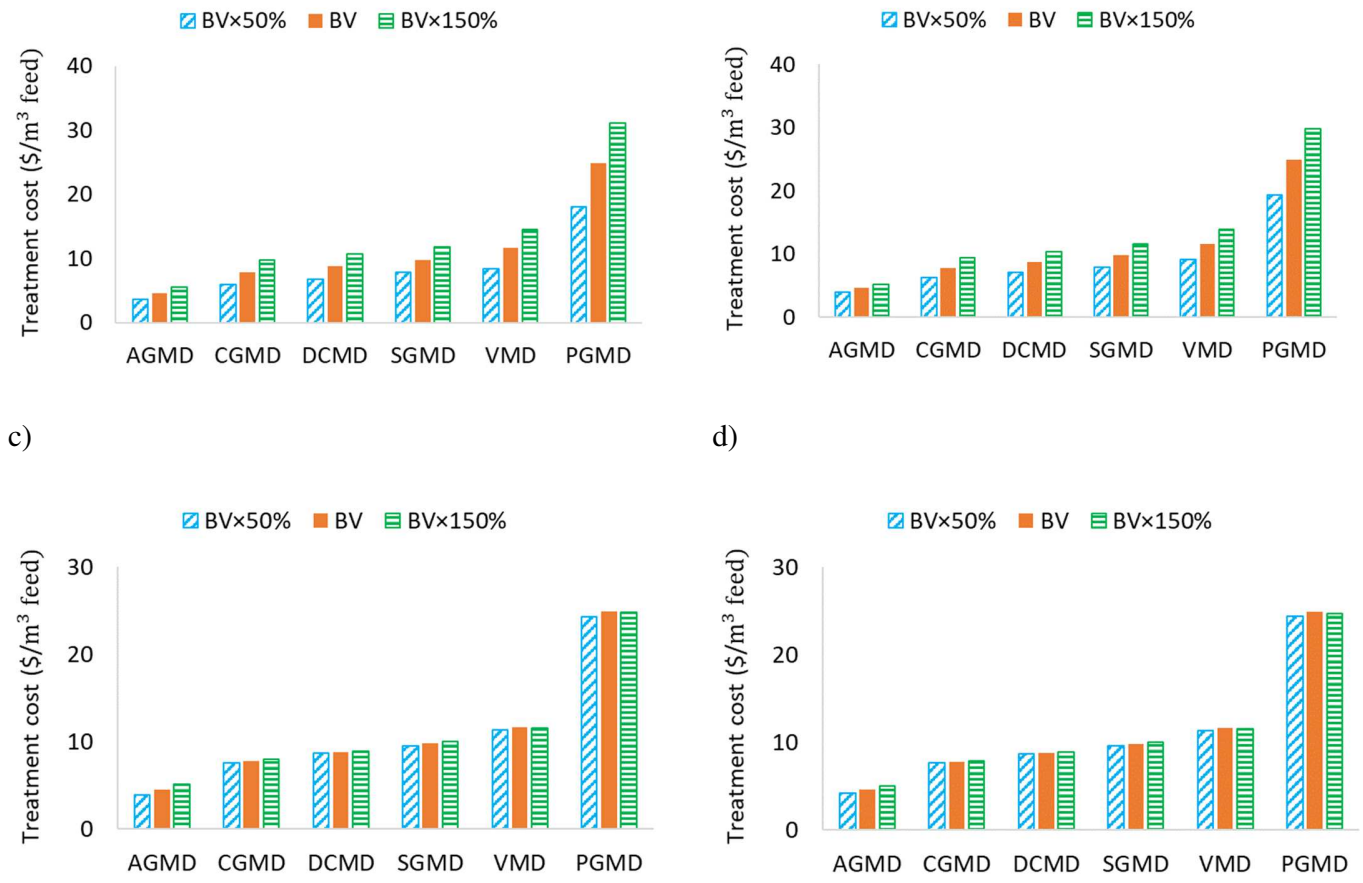

Figure A1. Variation in minimum treatment cost as a function of a) steam cost with baseline value (BV) of 0.008 ($/kg steam), b) electricity cost with baseline value of 0.069 ($/kWh) c) membrane and module costs with baseline values as specified in table A3, d) membrane replacement cost with baseline value of (17%/year)

Sensitivity analysis- Membrane properties: Figure A2 depicts the variation in optimum treatment costs as a function of membrane module properties (including membrane permeability coefficient, membrane effective thermal conductivity, and hydraulic diameter) as compared to the base line value (BV) of the costs considered in this study's main analysis. Hydraulic diameter is calculated using module channel height, spacer porosity, and filament diameter. As a result, rather than conducting individual sensitivity analyses on these parameters, we conducted sensitivity analysis on hydraulic diameter. Similarly, we conducted sensitivity analysis on the

effective thermal conductivity of the membrane rather than on the thermal conductivity of the membrane solid material and its porosity. The current sensitivity analysis is performed by multiplying the base line value of the above-mentioned properties by 50% and 150%. Regardless of changes in BV of membrane properties, the order of superiority of performance of various MD configurations remains constant, with AGMD outperforming all other configurations. Reduced membrane permeability (figure A2a) increases treatment costs in DCMD, CGMD, and PGMD due to increased mass transfer resistance and flux reduction. However, the treatment costs for AGMD, VMD, and SGMD remains approximately constant regardless of variation in membrane permeability. This is because mass transfer resistance is primarily determined by the air gap and air channel in AGMD and SGMD. In the case of VMD, the decrease in flux caused by a decrease in membrane permeability is offset by a decrease in vacuum pressure.

Reduced effective thermal conductivity reduces the treatment cost of DCMD, CGMD, and PGMD configurations due to the increase in thermal efficiency. However, the treatment cost of AGMD, SGMD, and VMD remains roughly constant as the thermal conductivity of the membrane decreases. This is because conduction is primarily controlled by the air gap, air channel, and vacuum channel in these configurations.

a)

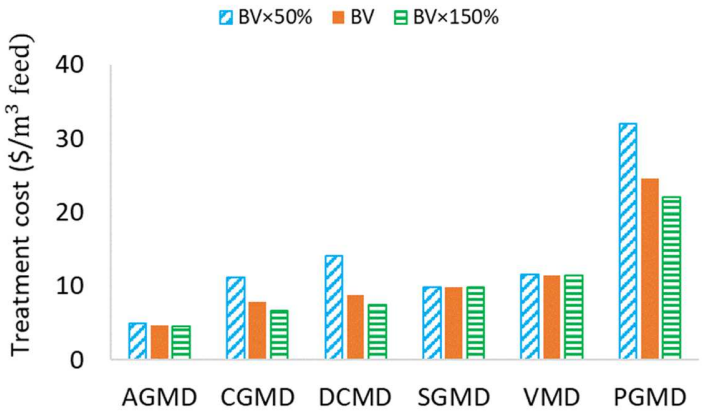
BV×50%
BV
BV×150%
Treatment cost ($/m³ feed)
40
30
20
10
0
AGMD
CGMD
DCMD
SGMD
VMD
PGMD

b)

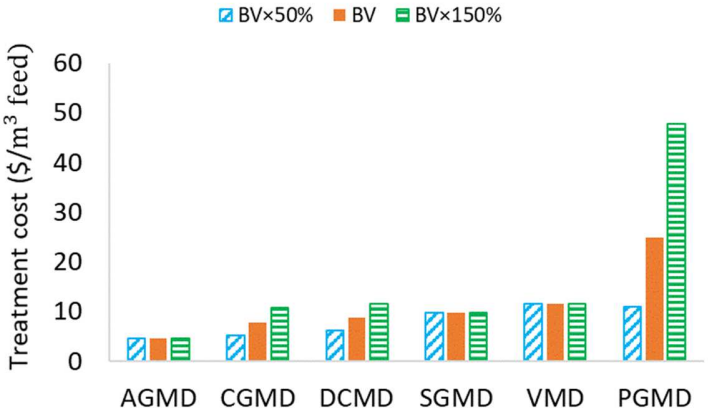
BV×50%
BV
BV×150%
Treatment cost ($/m³ feed)
60
50
40
30
20
10
0
AGMD
CGMD
DCMD
SGMD
VMD
PGMD

c)

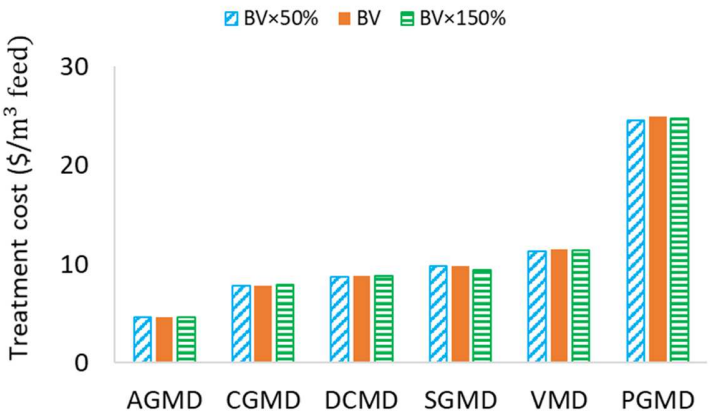

Figure A2. Variation in minimum treatment cost as a function of a) membrane permeability coefficient with baseline value (BV) of 0.94×10^{-10} $\left(\frac{\text{kg}}{\text{s.m.Pa}}\right)$, b) membrane effective thermal conductivity with baseline value of 0.055×10^{-3} $\left(\frac{\text{kW}}{\text{m.K}}\right)$ c) hydraulic diameter with baseline value of 2mm. The baseline values of effective thermal conductivity and hydraulic diameter are calculated using the parameters in table A2 and the correlations in table A7.